Accurate AoA Estimation for RFID Tag Array with Mutual Coupling

Zhongqin Wang, *Member, IEEE*, J. Andrew Zhang, *Senior Member, IEEE*,
Fu Xiao, *Member, IEEE*, Min Xu, *Member, IEEE*

***Abstract*—Angle-of-arrival (AoA) estimation is an important problem in passive RFID systems. Affixing an RFID tag array to an object enables to acquire its orientation information. However, the electromagnetic interaction between the tags can induce mutual coupling interference, distorting the RFID fingerprint measurements used for AoA estimation. Moreover, RFID reader modes with radio frequency (RF) noise-tolerant Miller encoding can induce π-radians phase jump. In this paper, we propose a scheme called RF-Mirror that can resolve the mutual coupling and phase jump problems and achieve accurate AoA estimation for an array with two or more tags. Firstly, we characterize the impact of mutual coupling on a tag's signal fingerprint and develop novel RSSI/phase-distance models. We then develop new experimental methods and signal processing techniques to verify the effectiveness of the proposed models. Based on the validated models, we develop new AoA estimation algorithms for tag arrays that deal with the mutual coupling effect explicitly. We provide extensive experimental results, which demonstrate that RF-Mirror can achieve significantly improved performance compared to baseline schemes, with median AoA estimation errors of 11.65° and 6.29° for two- and four-tag arrays, respectively.**

***Index Terms*—RFID, Mutual Coupling, Angle of Arrival, Tag Array, Phase Ambiguity, Radiation Pattern.**

I. Introduction

PASSIVE radio frequency identification (RFID) uses wireless signals to identify battery-free RFID tags, even in non-line-of-sight (NLOS) scenarios. Many commercial-off-the-shelf (COTS) readers can report each tag's backscatter signal fingerprint, including received signal strength indication (RSSI) and radio frequency (RF) phase, to indicate the distance relationship between a tag and a reader antenna. Recent studies [1]–[8] consider the use of an RFID tag array affixed on an object, while single-tag solutions only attach one RFID tag on a tracked object. In addition to estimating position information, the tag-array based solution can indicate the orientation of an RFID-tagged object by calculating the difference of phases between adjacent tags, called phase difference of arrival (PDoA).

In an RFID tag array, however, the *tag mutual coupling effect* is induced by the electromagnetic interaction among tags, thereby changing the radiation pattern (i.e., tag gains in different directions) and antenna impedance of each tag [9]–[11]. More intuitively, this effect can significantly impact the reading performance of the RFID system and distort the RSSI and RF phase measurements (as will be elaborated in Section II. A). Some previous methods [3], [12]–[14] may only measure the relative orientation change, meaning that the reported angle is not a real value of the tag array relative to a reader antenna. When performing localization, these methods may minimize the impact of tag mutual coupling by fusing RF phase measurements from multiple reader antennas. The works [9], [11] proposed an inductive coupling model to describe the change in the RFID signal amplitude (i.e., RSSI) due to the tag mutual coupling. However, this model cannot characterize the tag mutual coupling impact on the RF phase. The Angle of Arrival (AoA) estimation requires accurate RF phase measurement of each tag in the tag array to calculate PDoA. Tagyro [2] is the first system that deals with the coupling effect in PDoA-based orientation tracking, by using a virtual spacing between each pair of tags in the tag array. However, since the impact of tag mutual coupling on the RFID fingerprint is direction-dependent, Tagyro may not always work well. Hence, accurate AoA estimation in a tag-array based RFID system is still a challenging open problem.

In tag-array based AoA estimation, we still face the following two major challenges that need to be overcome.

1) RF phase model under tag mutual coupling: In AoA estimation, we need to calculate accurate PDoA values based on RF phase measurements. However, most existing tag array-based systems perform localization or orientation tracking using an ideal RF phase-distance model [7], [15], [16], which does not contain any terms to characterize the change in each tag's RFID fingerprint due to the tag mutual coupling effect. And the phase distortion for each tag element may be different, which cannot be directly removed in calculating PDoA.

2) π-radians phase jump: Some RF phase measurements may contain π-radians phase jumps, meaning that a reported RF phase may be the true value or the true value plus/minus π radians (as will be detailed in Section II. B). This phenomenon often happens when an RFID reader is set to the standard mode with Miller encoding, including 'Hybrid', 'Dense Reader M4', 'DenseReaderM4Two' and 'DenseReaderM8'. To remove the phase jump, we can directly perform a modulo-π operation on RF phase. However, since the processed phase is within $[0, \pi]$, the spacing between adjacent tags should be less than one-eighth wavelength (one-fourth wavelength corresponds to the RF phase range of $[0, 2\pi]$) to determine the unique AoA estimate. This tag-array setup with smaller spacing may decrease the AoA resolution and make the estimate sensitive to

Zhongqin Wang is with the College of Information and Engineering, Capital Normal University, Beijing 100048, China. (E-mail: zhongqin.wang@cnu.edu.cn)

J. Andrew Zhang and Min Xu (Corresponding Author) are with the School of Electrical and Data Engineering, University of Technology Sydney, Sydney 2007, Australia. (E-mail:{andrew.zhang, min.xu}@uts.edu.au)

Fu Xiao is with the College of Computer, Nanjing University of Posts and Telecommunications, Nanjing 21000, Jiangsu, China. (E-mail: xiaof@njupt.edu.cn)

measurement noise [17]. In addition, to our knowledge, most prior RFID systems work in the mode of 'Max Throughput' with FM0 encoding. This reader mode can provide a faster reading rate and is free from the impact of the π-radians phase jump. However, the RFID signal is very sensitive to RF noise interference and some tags may be harder to be read, especially in a scenario where multiple readers work at the same time. This problem has not been investigated in previous RFID sensing works.

In this work, we propose a scheme *RF-Mirror* that enables to accurately estimate the AoA of RFID signals received at a tag array from a reader antenna, in the presence of the mutual coupling effect and π-radians phase jump. RF-Mirror can work at FM0- and Miller-encoding reader modes. RF-Mirror is developed by taking into the mutual coupling effect account and then leveraging it to mitigate π-radians phase jump in AoA estimation. It allows the use of RFID arrays with tags spaced more flexibly, via addressing both the mutual coupling and phase estimation ambiguity issues. RF-Mirror is demonstrated to work well on various arrays built with two and more tags. Our main contributions are described as follows.

1) We develop novel phase- and RSSI-distance models for an RFID tag in a tag array with many new updates, including the introduction of mutual coupling characteristics and π-radians phase jump. Our models provide more accurate characterization for RFID signals received at a tag array.

2) We develop novel signal processing techniques to verify the proposed fingerprint models. Such procedure is conducted only using RSSI and RF phase measurements in the absence and presence of tag mutual coupling, respectively. We also propose several algorithms to estimate the parameters in our models, including tag hardware-related phase shift, tag radiation pattern and reflection coefficient. We conduct a series of validation experiments, which shows that the simulated RFID fingerprints can match well with the actually-measured ones.

3) We develop novel AoA estimation methods based on our models for multi-tag arrays, only using RFID fingerprint measurements. For a two-tag array, we develop an easy-to-implement method via decoupling the mutual coupling between tags. To achieve this, we pre-estimate some constant parameters independent of positions and directions of RFID tags relative to a reader antenna. Comparatively, decoupling in an array with more than two tags is more complicated since the tag mutual coupling effect induces much different impacts on each tag. It is challenging to estimate those constant terms like the two-tag array based solution. Instead, we propose a fingerprint matching method for AoA estimation, with the collection of prior knowledge of RFID fingerprints of all tags in pre-defined directions. These methods enable efficient removal of the mutual coupling effect and the π-radians phase ambiguity in AoA estimation.

4) We provide extensive experimental results to verify the effectiveness of our RF-Mirror scheme. RF-Mirror is shown to significantly outperform several baseline schemes, achieving the median AoA estimation errors of 11.65° and 6.29° on two- and four-tag arrays, respectively. The experiment also shows that RF-Mirror is robust to different multipath scenarios, tag array deployment, and tag types.

II. Preliminaries

This section demonstrates the tag mutual coupling effect and the π-radians phase jump problem.

A. Impact of tag mutual coupling

At first, we present an example to show the impact of tag mutual coupling on RSSI and RF phase. As shown in Fig. 1a, an Impinj E51 tag T_1 is fixed at the distance of 100 cm away from a reader antenna. Another tag T_2 of the same type is placed in parallel to T_1. The centers of the tags and the reader antenna are in the same plane. The operating frequency is 920.625 MHz. The reader mode is configured at 'Dense Reader M4'. We use a mod-π function to remove π-radians phase jump which will be described in detail in Section II. B. Each tag is written with a unique electronic product code (EPC) for identification. We read T_1 many times and calculate its average RSSI and RF phase.

The experiment results in Fig. 1b and Fig. 1c show the changes in the RSSI and RF phase for T_1, respectively. Among them, the two straight lines are the values measured in the absence of T_2 (we remove T_2 from the reading zone such that it has no effect on T_1). When T_2 is present near T_1 and is moved away from 2 cm to 40 cm at 1 cm spacing, the RSSI and RF phase for T_1 change significantly, i.e., they swing about and converge to the values when T_2 is absent. The results indicate that with tag mutual coupling in practical arrays or when tags are close to each other, the tag fingerprints may divert significantly from the ideal models without coupling. Thus, the impact of tag mutual coupling should be taken into account to get accurate AoA estimation.

B. Impact of π-radians phase jump

Let us look at another example to show the phenomenon of the π-radians phase jump. A COTS reader (e.g., Impinj R420 used in this experiment) is configured in all standard modes, including 'Max Throughput', 'Hybrid', 'Dense Reader M4', 'DenseReaderM4Two' and 'DenseReaderM8', respectively, to measure each tag's RF phase. The tag and reader antenna are respectively fixed at the same position each time.

The experiment result in Fig. 2 shows that except for 'Max Throughput', other reader modes all induce the π-radians phase jump. The 'Max Throughput' mode adopts a straightforward FM0 encoding at the tag end, making the reader more easily detect a tag state transition in each symbol [18]. The reader may take the RFID data stream into account to correct the phase jump. To our knowledge, most existing RFID works are generally configured in this mode. However, this mode is inefficient for suppressing RF noise interference, especially in the case that multiple readers work simultaneously, and some RFID tags may become unreadable. Thus, it is required to avoid using the mode 'Max Throughput' in practical applications according to [19]. Once the other mode with Miller encoding is selected, the π-radians phase jump will inevitably occur.

To focus on the impact of the π-radians phase jump, we ignore the tag mutual coupling effect for now. Let $\mathcal{P}_{T_1}$ and

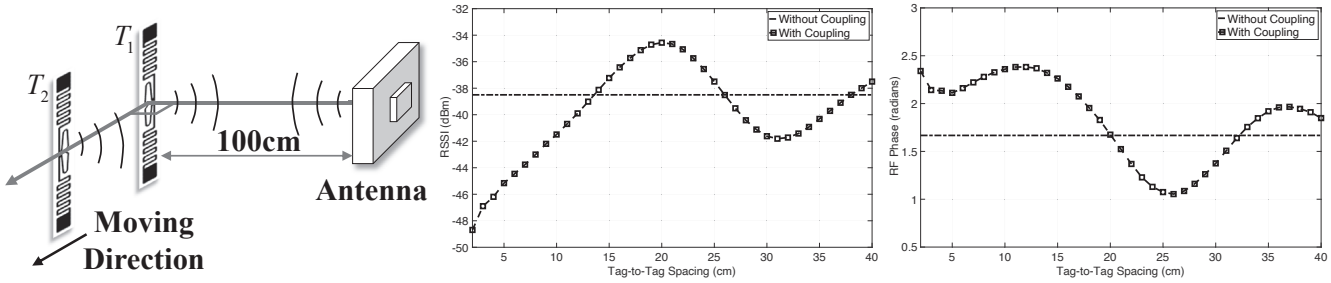

(a) Experiment setup (b) RSSI of the fixed tag T_1 over tag spacing (c) Phase of the fixed tag T_1 over tag spacing

Fig. 1: The impact of tag mutual coupling. Two tags T_1 and T_2 are assigned different EPCs for identification. The tag T_1 and the reader antenna are fixed. As T_2 moves away from T_1, the reported RSSI and RF phase for T_1 swing about and converge to the values when T_2 is absent in the reading zone.

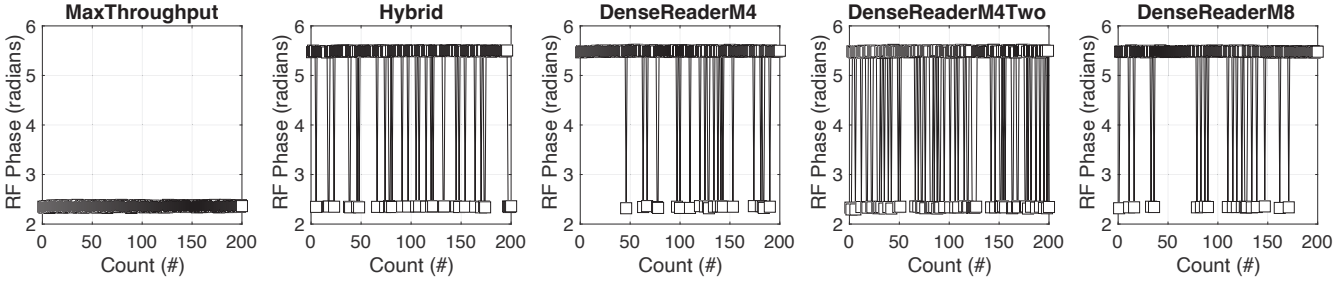

Fig. 2: The impact of π-radians phase jump. We configure a COTS reader in the standard reader modes of 'Max Throughput', 'Hybrid', 'Dense Reader M4', 'DenseReaderM4Two' and 'DenseReaderM8', respectively, to collect the RF phase of a tag at the same position. Except for 'Max Throughput', the π-radians phase jump happens in all the other modes.

$\mathcal{P}_{T_2}$ be the RF phase measurements of two RFID tags T_1 and T_2, λ be the carrier wavelength, D be the spacing between two adjacent tags. To resolve the potential π-radians phase jump in $\mathcal{P}_{T_1}$ and $\mathcal{P}_{T_2}$, we apply $\mathcal{P}'_{T_i} = \mathrm{mod}\left(\mathcal{P}_{T_i}, \pi\right)$, where $\mathrm{mod}\left(\cdot, \pi\right)$ is a modulo-π function to make the RF phase within the range of $[0, \pi]$. According to an ideal phase-distance model [6], [8], [20]–[22], the AoA θ is calculated based on PDoA,

$$\theta \approx \arccos\left[\frac{\lambda}{4\pi D}\left(\mathcal{P}'_{T_1} - \mathcal{P}'_{T_2} + \pi\Delta k\right)\right], \tag{1}$$

where Δk is an unknown integer. To remove its impact in AoA estimation, we have two possible solutions:

1) The spacing D is reduced to less than $\lambda/8$ (about 4 cm), then Δk can be uniquely determined by

$$\Delta k = \begin{cases} 1, & \left(\mathcal{P}'_{T_1} - \mathcal{P}'_{T_2}\right) \in \left[-\pi, -\frac{\pi}{2}\right) \\ 0, & \left(\mathcal{P}'_{T_1} - \mathcal{P}'_{T_2}\right) \in \left[-\frac{\pi}{2}, \frac{\pi}{2}\right) \\ -1, & \left(\mathcal{P}'_{T_1} - \mathcal{P}'_{T_2}\right) \in \left[\frac{\pi}{2}, \pi\right] \end{cases}, \tag{2}$$

However, compared to using a larger tag spacing (e.g., up to $\lambda/4$ corresponding to the RF phase range of $[0, 2\pi]$), this tag array setup has the following disadvantages. First, the AoA resolution will be decreased by 2 times, which means the AoA has twice the estimation uncertainty or error variance. Second, the estimation becomes more sensitive to the phase measurement noise [17]. Third, it will be harder for the tags to respond to an RFID reader due to the impact of tag mutual coupling, as will be shown in Fig. 21 in Section VIII.

2) Another solution is to obtain a prior knowledge of which tag is closer to a reader antenna, i.e., $d_{T_1} - d_{T_2} > 0$ or $d_{T_1} - d_{T_2} < 0$, where d_{T_1} and d_{T_2} are the distances of a reader antenna to T_1 and T_2, respectively. Given $D \leq \frac{\lambda}{4}$, we can uniquely determine the integer Δk using the triangle rule that the absolute difference between the lengths of two sides is smaller than the length of the third side,

$$\Delta k = \begin{cases} 1, & \left(\mathcal{P}'_{T_1} - \mathcal{P}'_{T_2}\right) \in [-\pi, 0), d_{T_1} - d_{T_2} > 0 \\ 0, & \left(\mathcal{P}'_{T_1} - \mathcal{P}'_{T_2}\right) \in [-\pi, 0), d_{T_1} - d_{T_2} < 0 \\ 0, & \left(\mathcal{P}'_{T_1} - \mathcal{P}'_{T_2}\right) \in [0, \pi], d_{T_1} - d_{T_2} \geq 0 \\ -1, & \left(\mathcal{P}'_{T_1} - \mathcal{P}'_{T_2}\right) \in [0, \pi], d_{T_1} - d_{T_2} \leq 0 \end{cases}, \tag{3}$$

Unfortunately, it is not always possible to have the prior knowledge, particularly when the tag array moves over time in a dynamic environment. Furthermore, the tag mutual coupling effect makes this problem more challenging, as the distancxe estimation becomes harder.

To achieve fine-grained AoA estimation, we need to suppress the impact of tag mutual coupling and calculate accurate PDoA under the tag separation distance of up to $\lambda/4$.

III. Overview of the RF-Mirror Scheme

Our scheme RF-Mirror deals with the tag mutual coupling effect in an RFID tag array to estimate the AoA of the backscattered signals received at the array in COTS RFID systems. RF-Mirror solves the two critical problems as described previously: the mutual coupling effect and the π-radians phase jump. At a high level, RF-Mirror models the mutual coupling and leverages it to remove the π-radians phase jump in AoA estimation. This work includes the following parts:

Tag Mutual Coupling Modeling. When multiple RFID tags are present in a reading zone, the signal fingerprint

of a responding tag (only one tag responds at a time for anti-collision) can be impacted by its nearby tags, which is generally ignored in the prior signal modeling. In RF-Mirror, we take into account the electromagnetic interference from those silent tags and then build backscatter signal fingerprint models. The updated models could characterize the impact of the tag mutual coupling on RSSI and RF phase.

RFID Fingerprint Model Verification. The modeling verification process is conducted based on a two-tag array (in an array with more tags, since the tag mutual coupling effect is different on each tag, it may make the model verification more complicated). We first collect RFID fingerprints of each tag in the non-coupling and coupling cases, respectively. Based on these measurements, we then develop novel experiment methods and signal processing techniques for modeling verification.

Decoupling for Unambiguous AoA Estimation. We develop two AoA estimation algorithms for the RFID arrays with two and more tags. The former performs only using RFID fingerprints in the coupling case, while the latter requires prior knowledge of RFID fingerprints in pre-defined directions.

In Section IV, Section V, and Section VI, we describe each part in detail.

IV. Tag Mutual Coupling Modeling

This section analyzes the signal propagation characteristics of an RFID tag of being inventoried in a multi-tag scenario, and then develops novel RFID fingerprint models based on the analysis of the channel frequency response (CFR).

A. RFID signal propagation in multi-tag scenario

Let us consider a scenario shown Fig. 3 where there exists a responding tag $\boldsymbol{T}$ and other RFID tags T_i in front of a reader A in a practical environment. In RFID systems, only one RFID tag responds in an inventory, while other tags wait for responding to avoid signal collision. At a responding time, an RFID reader mainly receives four types of RFID signals [23] as described below.

Self-Jamming Signals. The signals are induced by the transmit leakage and static environment clutter. To minimize an RFID system's cost and complexity, most COTS readers work with monostatic antennas that enable simultaneous transmission of continuous wave (CW) signals and receive the backscatter CW signals from RFID tags. There always exists a leakage signal propagating from the transmitter A_T to receiver A_R of the reader. And static objects such as chairs, floor, wall, furniture, and all other clutter in a practical environment can also reflect the transmitted signal to A_R. These signals are generally time-invariant. According to [23], [24], an adaptive receiver or filter can be applied to suppress the impact of these self-jamming signals, which can be ignored in our modeling.

Direct Propagation Signal. This refers to the CW signal directly traveling from A_T to $\boldsymbol{T}$ in the line-of-sight (LOS) propagation, and then scattered back from $\boldsymbol{T}$ to A_R in the same path after $\boldsymbol{T}$ responds (i.e., $A_T \rightarrow \boldsymbol{T} \rightarrow A_R$). The complex-valued CFR of this direct propagation signal is denoted as $h_{A_T,\boldsymbol{T},A_R}$.

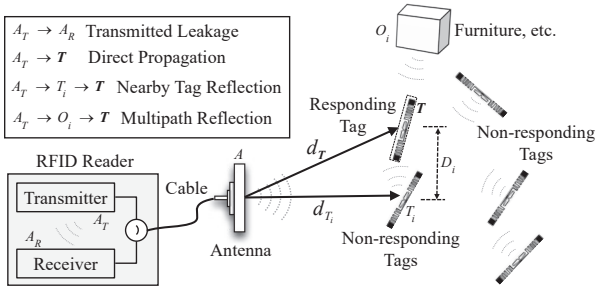

Fig. 3: RFID signal propagation paths

Nearby Tag Reflection Signals. Since RFID tags almost simultaneously power up, the electromagnetic field from other non-responding tags has an important impact on that of $\boldsymbol{T}$ and thereby results in the mutual coupling effect. We can regard it as $\boldsymbol{T}$ receives some signals emitted from each RFID tag T_i [2]. The corresponding backscatter signals may include two reflection paths $A_T \rightarrow T_i \rightarrow \boldsymbol{T} \rightarrow A_R$ and $A_T \rightarrow T_i \rightarrow \boldsymbol{T} \rightarrow T_i \rightarrow A_R$. The latter path has the longer propagation distance, so it contains signals with much smaller power and then we ignore their impacts in this work. Thus, the CFR of the CW signal reflected off a nearby tag T_i is expressed as $h_{A_T,T_i,\boldsymbol{T},A_R}$.

Multipath Signals. In an actual environment, some objects reflect the transmitted signal from A_T to RFID tags and the backscatter signals back to A_R. The CFR caused by the environment multipath is denoted as $h_{\mathbb{N}}$.

Let $\boldsymbol{H}$ be the total CFR of the received CW signals at the reader receiver, then we have

$$\begin{aligned}\boldsymbol{H} =& h_{A_T,\boldsymbol{T},A_R} + \sum_i h_{A_T,T_i,\boldsymbol{T},A_R} + h_{\mathbb{N}} \\ =& \underbrace{h_{A_T} h_{A_T,\boldsymbol{T}} h_{\boldsymbol{T}} h_{\boldsymbol{T},A_R} h_{A_R}}_{A_T \rightarrow \boldsymbol{T} \rightarrow A_R} + \underbrace{\sum_i h_{A_T} h_{A_T,T_i,\boldsymbol{T}} h_{T_i} h_{\boldsymbol{T}} h_{\boldsymbol{T},A_R} h_{A_R}}_{A_T \rightarrow T_i \rightarrow \boldsymbol{T} \rightarrow A_R} + h_{\mathbb{N}} \\ =& h_A \underbrace{\left(h_{A_T,\boldsymbol{T}} + \sum_i h_{T_i} h_{A_T,T_i,\boldsymbol{T}} \right)}_{forward\ link} \underbrace{h_{\boldsymbol{T}} h_{\boldsymbol{T},A_R}}_{reverse\ link} + h_{\mathbb{N}}\end{aligned} \tag{4}$$

In the above equation, each component is described below.

1) h_A is the CFR associated with the reader antenna, cable and reader circuit. Here $h_A = h_{A_T} h_{A_R} = \rho_A e^{-\boldsymbol{J}\phi_A}$, where h_{A_T} and h_{A_R} represent the CFR of the transmitter and receiver, respectively. The terms ρ_A, ϕ_A and $\boldsymbol{J}$ represent amplitude, phase shift, and imaginary unit, respectively.

2) $h_{\boldsymbol{T}}$ and h_{T_i} denote the tag hardware characteristics of the responding tag $\boldsymbol{T}$ and the silent tag T_i in the presence of mutual coupling, respectively,

$$\begin{cases} h_{\boldsymbol{T}} = \rho_{\boldsymbol{T}} e^{-\boldsymbol{J}(\phi_{\boldsymbol{T}} + \pi)} \\ h_{T_i} = \epsilon_{T_i} e^{-\boldsymbol{J}\left(\phi_{T_i} + \pi\right)} \end{cases}, \tag{5}$$

where $\rho_{\boldsymbol{T}}$ is the modulation factor when $\boldsymbol{T}$ switches between the states 'A' and 'B' (i.e., the 'more-reflective' and 'less-reflective' states at different reflection power levels [25]). And ϵ_{T_i} is the reflection coefficient of T_i. When $\boldsymbol{T}$ transmits a backscatter signal back to the reader receiver, an approximate short circuit is presented on the tag (a true short circuit cannot

be achieved in practice). At this moment, the silent tag T_i is in an open circuit condition. In the short- and open- circuit cases, the transmitted signals reflected to A_R from $\boldsymbol{T}$ and reflected to $\boldsymbol{T}$ from T_i will both introduce a π-radians phase shift [26]. In addition, there exist a phase shift caused by the tag hardware characteristic, i.e., $\phi_{\boldsymbol{T}}$ and ϕ_{T_i}. For tags of the same type, we assume that $\phi_T = \phi_{\boldsymbol{T}} = \phi_{T_i}$ in this work.

3) $h_{A_T,\boldsymbol{T}}$ and $h_{\boldsymbol{T},A_R}$ represent the CFR of the CW signal traveling along the forward and reverse propagation paths, respectively, while $h_{A_T,T_i,\boldsymbol{T}}$ denotes the CFR of the signal propagating along the reflected path off a nearby tag,

$$\begin{cases} h_{A_T,\boldsymbol{T}} = h_{\boldsymbol{T},A_R} = \dfrac{\mu_{A,\boldsymbol{T}} G_A G_{\boldsymbol{T}}}{d_{\boldsymbol{T}}} e^{-\boldsymbol{J}\left(\frac{2\pi}{\lambda} d_{\boldsymbol{T}} + \theta_{A,\boldsymbol{T}}\right)} \\ h_{A_T,T_i,\boldsymbol{T}} = \dfrac{\mu_{A,T_i}\mu_{T_i,\boldsymbol{T}} G_A G_{T_i} G_{T_i,\boldsymbol{T}} G_{\boldsymbol{T},T_i}}{d_{T_i} + D_{T_i,\boldsymbol{T}}} e^{-\boldsymbol{J}\left[\frac{2\pi}{\lambda}\left(d_{T_i} + D_{T_i,\boldsymbol{T}}\right) + \theta_{A,T_i} + \theta_{T_i,\boldsymbol{T}}\right]} \end{cases}, \tag{6}$$

where $d_{\boldsymbol{T}}$ and d_{T_i} are the distances from $\boldsymbol{T}$ and T_i to A, respectively; $D_{T_i,\boldsymbol{T}}$ is the distance between $\boldsymbol{T}$ and T_i; G_A is the reader antenna gain; $G_{\boldsymbol{T}}$ (and G_{T_i}) is the tag antenna gain in the direction of $\boldsymbol{T}$ (and T_i) relative to A; $G_{T_i,\boldsymbol{T}}$ (and $G_{\boldsymbol{T},T_i}$) is the tag antenna gain in the direction of T_i towards $\boldsymbol{T}$ (and $\boldsymbol{T}$ towards T_i); $\{\mu_{A,\boldsymbol{T}}, \theta_{A,\boldsymbol{T}}\}$ (and $\{\mu_{A,T_i}, \theta_{A,T_i}\}$) are the polarization terms in the amplitude and phase shift between A and $\boldsymbol{T}$ (and T_i), while $\{\mu_{T_i,\boldsymbol{T}}, \theta_{T_i,\boldsymbol{T}}\}$ are the ones between T_i and $\boldsymbol{T}$. *Note that the amplitude expression is derived from the Friis equation [27] in the unit of the voltage ratio rather than in dB (See Eq.* (10)*).*

Substituting these variables into Eq. (4), the CFR $\boldsymbol{H}$ can be rewritten as

$$\boldsymbol{H} = \rho_{\boldsymbol{H}} e^{-\boldsymbol{J}\phi_{\boldsymbol{H}}} \left(1 + \sum_{T_i \neq \boldsymbol{T}} \alpha_{T_i,\boldsymbol{T}} e^{-\boldsymbol{J}\beta_{T_i,\boldsymbol{T}}}\right) + h_{\mathbb{N}}, \tag{7}$$

where

$$\begin{cases} \rho_{\boldsymbol{H}} = \rho_A \rho_{\boldsymbol{T}} \left(\dfrac{\mu_{A,\boldsymbol{T}} G_A G_{\boldsymbol{T}}}{d_{\boldsymbol{T}}}\right)^2 \\ \phi_{\boldsymbol{H}} = \dfrac{4\pi}{\lambda} d_{\boldsymbol{T}} + 2\theta_{A,\boldsymbol{T}} + \phi_A + \phi_T + \pi \\ \alpha_{T_i,\boldsymbol{T}} = \dfrac{\mu_{A,T_i}\mu_{T_i,\boldsymbol{T}} \epsilon_{T_i} G_{T_i} G_{T_i,\boldsymbol{T}} G_{\boldsymbol{T},T_i} d_{\boldsymbol{T}}}{\mu_{A,\boldsymbol{T}} G_{\boldsymbol{T}} \left(d_{T_i} + D_{T_i,\boldsymbol{T}}\right)} \\ \beta_{T_i,\boldsymbol{T}} = \dfrac{2\pi}{\lambda}\left(d_{T_i} + D_{T_i,\boldsymbol{T}} - d_{\boldsymbol{T}}\right) + \theta_{A,T_i} - \theta_{A,\boldsymbol{T}} + \theta_{T_i,\boldsymbol{T}} + \phi_T + \pi \end{cases}. \tag{8}$$

In the following, we will introduce how to derive novel RSSI and RF phase models from the CFR $\boldsymbol{H}$ in the presence of the mutual coupling effect and the π-radians phase jump.

B. Our RSSI and RF phase models

Let $\mathcal{R}^t$ be the transmitted power of a COTS RFID reader in the unit of *dBm*, $\mathcal{R}^r_{\boldsymbol{T}}$ be the received power (i.e., *RSSI*) in dBm, and $\mathcal{P}_{\boldsymbol{T}}$ be the reported *RF phase* in the unit of radians within the range of $[0, 2\pi]$. In this subsection, we propose new RSSI- and phase-distance models to represent these measured RFID fingerprints. The models will be verified in Section V. *For simplicity, we ignore the multipath term $h_{\mathbb{N}}$ in the following, but its impact on AoA estimation will be validated in our experiment evaluation.*

RSSI-distance model. Given the voltages V^t and $V^r_{\boldsymbol{T}}$ of the transmitted and received signals in *volts*, we use the modulus function $\|\cdot\|$ to get the amplitude of the complex number $\boldsymbol{H}$,

$$\|\boldsymbol{H}\| = \frac{V^r_{\boldsymbol{T}}}{V^t} = \rho_A \rho_{\boldsymbol{T}} \left(\frac{G_A G_{\boldsymbol{T}} \mu_{A,\boldsymbol{T}}}{d_{\boldsymbol{T}}}\right)^2 \Gamma_{\boldsymbol{T}}, \tag{9}$$

where $\Gamma_{\boldsymbol{T}} = \left\| 1 + \sum_{T_i \neq \boldsymbol{T}} \alpha_{T_i,\boldsymbol{T}} e^{-\boldsymbol{J}\beta_{T_i,\boldsymbol{T}}} \right\|$ is the tag mutual coupling term of RSSI, called as ***coupling RSSI*** in this paper. Recall that the power is proportional to the square of the voltage. Given the transmitted and received powers P^t and $P^r_{\boldsymbol{T}}$ in *watts*, we rewrite Eq. (9) in *DeciBels (dB)*,

$$\|\boldsymbol{H}\|^{dB} = 10 \log \frac{V^r_{\boldsymbol{T}}}{V^t} = 10 \log \left(\frac{P^r_{\boldsymbol{T}}}{P^t}\right)^{\frac{1}{2}}. \tag{10}$$

According to the transformation relationship between *dBm* and *watts*, we have $\mathcal{R}^r_{\boldsymbol{T}} - \mathcal{R}^t = 10 \log\left(P^r_{\boldsymbol{T}}/P^t\right)$. Thus, the RSSI-distance model in the linear scale is

$$10^{\frac{\mathcal{R}^r_{\boldsymbol{T}} - \mathcal{R}^t}{20}} = \rho_A \rho_{\boldsymbol{T}} \left(\frac{G_A G_{\boldsymbol{T}} \mu_{A,\boldsymbol{T}}}{d_{\boldsymbol{T}}}\right)^2 \Gamma_{\boldsymbol{T}}. \tag{11}$$

RF Phase-distance Model. The phase shift of $\boldsymbol{H}$ is approximately equal to the actually-measured RF phase $\mathcal{P}_{\boldsymbol{T}}$,

$$\mathcal{P}_{\boldsymbol{T}} = \operatorname{mod}\left[-\left(\frac{4\pi}{\lambda} d_{\boldsymbol{T}} + 2\theta_{A,\boldsymbol{T}} + \phi_A + \phi_T\right) + \Theta_{\boldsymbol{T}},\ 2\pi\right], \tag{12}$$

where $\Theta_{\boldsymbol{T}} = \angle\left(1 + \sum_{T_i \neq \boldsymbol{T}} \alpha_{T_i,\boldsymbol{T}} e^{-\boldsymbol{J}\beta_{T_i,\boldsymbol{T}}}\right)$ is the tag mutual coupling term of RF phase, named as ***coupling phase shift***, and the function $\angle\cdot$ is to obtain the phase shift of a complex number.

Further, we conduct an RF phase transformation to eliminate the π-radians phase jump using $\mathcal{P}'_{\boldsymbol{T}} = \operatorname{mod}\left(\mathcal{P}_{\boldsymbol{T}},\ \pi\right)$. Then the proposed phase-distance model is

$$\mathcal{P}'_{\boldsymbol{T}} = \operatorname{mod}\left[-\left(\frac{4\pi}{\lambda} d_{\boldsymbol{T}} + 2\theta_{A,\boldsymbol{T}} + \phi_A + \phi_T\right) + \Theta_{\boldsymbol{T}},\ \pi\right], \tag{13}$$

Discussion. Since RSSI has a lower distance resolution than RF phase and is highly relevant to the unknown reader antenna gain in each direction, it has not been widely used in most recently RFID works. However, the proposed RSSI model reveals that RSSI also suffers from the impact of the mutual coupling. Moreover, each RFID tag antenna gain in an array will be modified in different directions [28]. Our verification experiment is shown in Section V. D. Thus, RSSI becomes a direction-dependent parameter, providing a potential benefit to AoA estimation. In our scheme, the novelty is to combine RSSI and RF phase measurements for all tags in an array to achieve fine-grained AoA estimation, detailed in Section VI.

C. Comparison to state-of-the-art

Ideal RFID fingerprint model. For comparison, we use the defined variables above to rewrite the ideal RSSI and RF

phase models [6], [8], [20]–[22] as

$$\begin{cases} 10^{\frac{\mathcal{R}_{\boldsymbol{T}}^r - \mathcal{R}^t}{20}} = \rho_A \rho_{\boldsymbol{T}} \left(\dfrac{G_A G_{\boldsymbol{T}}}{d_{\boldsymbol{T}}} \right)^2 \\ \mathcal{P}_{\boldsymbol{T}} = \mathrm{mod}\left(\dfrac{4\pi}{\lambda} d_{\boldsymbol{T}} + \phi_A + \phi_T, 2\pi \right) \end{cases}. \tag{14}$$

Our proposed fingerprint models have the following updates:

1) Tag mutual coupling. When multiple RFID tags are closely placed, the impact of tag mutual coupling on RFID signal fingerprints cannot be ignored. Our models introduce the coupling terms and can characterize the changes in RSSI and RF phase due to the coupling;

2) π-radians phase jump. Our RF phase model considers the π-radians phase jump problem that associates with practical RFID operating modes with Miller encoding. Such a phase jump is required to be removed by the $\mathrm{mod}(\cdot, \pi)$ operation, in conjunction with the mutual coupling modeling. However, this operation accordingly introduces the π-radians phase ambiguity, making AoA estimation even other RFID sensing tasks become more challenging;

3) RF phase reversal. We use the negative sign of the phase in Eq. (13) to account for the fact that the reported RF phase by COTS readers decreases when a tag moves away from a reader antenna, as reported in prior experiments [29]. In fact, most RFID readers do not correct raw RF phase, so $-\mathcal{P}_{\boldsymbol{T}}$ should be used to describe the relationship between the RF phase and the distance traveled by the RFID signal;

4) Polarization mismatch. The existing models do not include any terms that indicate the impact of polarization. However, many works [13], [30], [31] observed that the RF phase/RSSI is a function of the direction of a tag relative to a reader antenna. Our models introduce such polarization mismatch terms to present the impact of polarization;

5) Tag reflection characteristic. Since a tag reflects the transmitted signal from an antenna transmitter back to the antenna receiver, the backscattered signal will be additionally shifted by π radians. In this case, the existing phase model should contain a phase shift of π radians. In our model, it is removed by the $\mathrm{mod}(\cdot, \pi)$ operation.

Electromagnetic field model. Some previous works (e.g., Twins [9], Trio [32], and Hu-Fu [11]) apply electromagnetic (EM) theory to describe the principle of tag mutual coupling. The EM field interaction between RFID tags produces a mutual impedance on each tag antenna and thereby introduces an additional voltage source. In this case, the voltage and current of each RFID tag are changed compared to the case in the absence of tag mutual coupling. The main differences between our work and the EM model are highlighted below.

1) Modeling theory. Our work analyzes the impact of tag mutual coupling based on signal processing theory and uses the CFR to characterize the changes in the amplitude and phase of the RFID backscatter signal. To our best knowledge, most COTS RFID readers cannot measure the voltage and current of an RFID tag, but can report the amplitude (i.e., RSSI) and phase values. Since RFID sensing systems mainly handles tag fingerprint measurements, our models can be directly applied into the existing works to improve the performance of tag-array based sensing systems.

2) RF phase. The existing EM model can only analyze the change in the backscatter power (i.e., RSSI) but fails to model the impact of tag mutual coupling on the RF phase. However, accurate RF phase measurements are required for phased array based AoA estimation. Our models can mitigate the phase offsets in RF phase caused by the coupling effect in PDoA measurements.

V. RFID Fingerprint Model Verification

In this section, we build a two-RFID-tag array and then verify our fingerprint models by comparing the actual measurements with the simulated values.

A. Simplified Models in two-RFID-tag array

In a two-tag array with the tags T_1 and T_2, if T_1 is responding, the coupling RSSI Γ_{T_1} and coupling phase shift Θ_{T_1} of T_1 described in Eq. (9) and Eq. (12) are simplified as

$$\begin{cases} \Gamma_{T_1} = \left\| 1 + \alpha_{T_2,T_1} e^{-\boldsymbol{J}\beta_{T_2,T_1}} \right\| \\ \Theta_{T_1} = \angle\left(1 + \alpha_{T_2,T_1} e^{-\boldsymbol{J}\beta_{T_2,T_1}} \right) \end{cases}. \tag{15}$$

For simplicity, let $\alpha_{T_1} = \alpha_{T_2,T_1}$ and $\beta_{T_1} = \beta_{T_2,T_1}$ in the following. Similarly, when T_2 is responding, let $\alpha_{T_2} = \alpha_{T_1,T_2}$ and $\beta_{T_2} = \beta_{T_1,T_2}$. In this case, Γ_{T_i} and Θ_{T_i} for a responding tag T_i ($\forall i = 1, 2$) are rewritten as

$$\begin{cases} \Gamma_{T_i} = \sqrt{1 + 2\alpha_{T_i} \cos\beta_{T_i} + {\alpha_{T_i}}^2}, & \text{(16a)} \\ \Theta_{T_i} = \arctan\left(\dfrac{-\alpha_{T_i} \sin\beta_{T_i}}{1 + \alpha_{T_i} \cos\beta_{T_i}} \right) + \pi k_{T_i}, & \text{(16b)} \end{cases}$$

where k_{T_i} is an unknown integer.

When the two tags are placed in parallel in the array, the polarization terms in RSSI and RF phase have the following relationship between the tags,

$$\begin{cases} \mu_{A,T_1} = \mu_{A,T_2} \\ \mu_{T_1,T_2} = \mu_{T_2,T_1} = 1 \\ \theta_{A,T_1} = \theta_{A,T_2} \\ \theta_{T_1,T_2} = \theta_{T_2,T_1} = 0 \end{cases}. \tag{17}$$

And when the two RFID tags are the same type, they have the same chip load and antenna impedances and the coupling effect induces the same mutual impedance on each tag. Thus, the impedance-related reflection coefficient and modulation factor of the tags are the same, i.e.,

$$\begin{cases} \epsilon_T = \epsilon_{T_1} \approx \epsilon_{T_2} \\ \rho_T = \rho_{T_1} \approx \rho_{T_2} \end{cases}. \tag{18}$$

According to Eq. (8), we then simplify $\{\alpha_{T_i}, \beta_{T_i}\}$ of T_1 and T_2 as

$$\begin{cases} \alpha_{T_1} = \dfrac{\epsilon_T G_{T_2,T_1} G_{T_1,T_2} G_{T_2}}{G_{T_1}} \dfrac{d_{T_1}}{d_{T_2} + D} \\ \alpha_{T_2} = \dfrac{\epsilon_T G_{T_1,T_2} G_{T_2,T_1} G_{T_1}}{G_{T_2}} \dfrac{d_{T_2}}{d_{T_1} + D} \end{cases}, \tag{19}$$

and

$$\begin{cases} \beta_{T_1} = \dfrac{2\pi}{\lambda} \left(d_{T_2} + D - d_{T_1} \right) + \phi_T + \pi \\ \beta_{T_2} = \dfrac{2\pi}{\lambda} \left(d_{T_1} + D - d_{T_2} \right) + \phi_T + \pi \end{cases}, \tag{20}$$

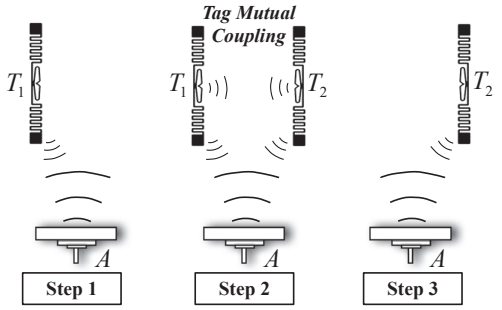

Fig. 4: Collecting RFID signal fingerprints in the absence and presence of tag mutual coupling for model verification.

where D is the spacing between T_1 and T_2. In the following, we mainly exploit the simplified models for verification.

B. Collecting RFID signal fingerprints for verification

We collect RSSI and RF phase measurements in the absence and presence of the tag mutual coupling effect for RFID fingerprint model verification. The experiment was conducted in free space with negligible multipath interference, and the collection process is shown in Fig. 4. Each tag is read several times at the same transmitted power and frequency, and the averaged values of RSSI and RF phase are used.

Step 1. At first, an RFID tag T_1 is placed in the reading region. Its measured RSSI and RF phase are denoted as $\{\overline{\mathcal{R}}^r_{T_1}, \overline{\mathcal{P}}_{T_1}\}$. Since no other tags are besides it, T_1 is free from the tag mutual coupling effect.

Step 2. Another tag T_2 is then placed besides T_1 to induce tag mutual coupling. The measured RSSI and RF phase of T_1 and T_2 are $\{\mathcal{R}^r_{T_1}, \mathcal{P}_{T_1}\}$ and $\{\mathcal{R}^r_{T_2}, \mathcal{P}_{T_2}\}$, respectively.

Step 3. Finally, we remove T_1 from the reading region. The measured RSSI and RF phase of T_2 in the absence of tag mutual coupling are expressed as $\{\overline{\mathcal{R}}^r_{T_2}, \overline{\mathcal{P}}_{T_2}\}$.

Specifically, the π-radians phase jump in these RF phase are removed by the modulo operation, and we have $\overline{\mathcal{P}}'_{T_i} = \mathrm{mod}\left(\overline{\mathcal{P}}_{T_i},\ \pi\right)$ and $\mathcal{P}'_{T_i} = \mathrm{mod}\left(\mathcal{P}_{T_i},\ \pi\right)$. In addition, it is easy to derive the RSSI and RF phase models in the non-coupling scenario that do not contain any coupling terms,

$$\begin{cases} 10^{\frac{\overline{\mathcal{R}}^r_{T_i} - \mathcal{R}^t}{20}} = \rho_A \overline{\rho}_{T_i} \left(\dfrac{\mu_{A,T_i} G_A \overline{G}_{T_i}}{d_{T_i}} \right)^2, & \text{(21a)} \\ \overline{\mathcal{P}}'_{T_i} = \mathrm{mod}\left[-\left(\dfrac{4\pi}{\lambda} d_{T_i} + 2\theta_{A,T_i} + \phi_A + \phi_T \right),\ \pi \right], & \text{(21b)} \end{cases}$$

where the terms $\overline{\rho}_{T_i}$ and $\overline{G}_{T_i}$ are the modulation factor and tag radiation pattern, which are different from those in the coupling case due to the tag mutual coupling effect.

C. Estimating tag hardware-related phase shift

The following aims to estimate the phase shift ϕ_T caused by the tag hardware based on the proposed fingerprint models.

At first, we divide RSSIs of the two tags in the coupling case to remove a series of variables (including ρ_A, ρ_T, G_A, and $\mu_{A,T}$) and we have

$$10^{\frac{R^r_{T_1} - R^r_{T_2}}{20}} = \left(\frac{G_{T_1} d_{T_2}}{G_{T_2} d_{T_1}} \right)^2 \frac{\Gamma_{T_1}}{\Gamma_{T_2}}. \quad (22)$$

Based on this, the optimal tag hardware-related phase shift ϕ_T can be estimated by finding the minimum residual,

$$\arg\min_{\phi_T \in [0, 2\pi]} \left| \left[\frac{G_{T_1}(\phi_T)\, d_{T_2}}{G_{T_2}(\phi_T)\, d_{T_1}} \right]^2 \frac{\Gamma_{T_1}(\phi_T)}{\Gamma_{T_2}(\phi_T)} - 10^{\frac{R^r_{T_1} - R^r_{T_2}}{20}} \right|, \quad (23)$$

where $\frac{d_{T_2}}{d_{T_1}} = 10^{\frac{\overline{\mathcal{R}}^r_{T_1} - \overline{\mathcal{R}}^r_{T_2}}{40}}$, which is calculated based on Eq. (21a). In the following, let us describe how to use RF phase measurements in the coupling and non-coupling cases to calculate $\frac{G_{T_1}(\phi_T)}{G_{T_2}(\phi_T)}$ and $\frac{\Gamma_{T_1}(\phi_T)}{\Gamma_{T_2}(\phi_T)}$ for a given ϕ_T.

1) Tag Gain Ratio $\frac{G_{T_1}(\phi_T)}{G_{T_2}(\phi_T)}$. According to Eq. (13) and Eq. (21b), the coupling phase shift Θ_{T_i} is obtained by subtracting the measured phase in the coupling and non-coupling cases,

$$\Theta_{T_i} = \mathrm{mod}\left(\mathcal{P}'_{T_i} - \overline{\mathcal{P}}'_{T_i}, \pi \right). \quad (24)$$

And the distance difference between the two tags is

$$d_{T_1} - d_{T_2} = \frac{\lambda}{4\pi} \left(\overline{\mathcal{P}}'_{T_2} - \overline{\mathcal{P}}'_{T_1} + \pi \Delta k_d \right), \quad (25)$$

where an integer Δk_d is determined as follows. Since the tag separation D is pre-specified within the length of $\lambda/4$ ($D \leq 8$ cm) and the sign of $(d_{T_1} - d_{T_2})$ is known by our manual measurement, we rely on Eq. (3) to determine Δk_d.

For a given ϕ_T, we first use $(d_{T_1} - d_{T_2})$ and D to calculate $\beta_{T_i}(\phi_T)$ based on Eq. (20). We then apply it and the calculated Θ_{T_i} into Eq. (16b) to calculate $\alpha_{T_i}(\phi_T)$,

$$\alpha_{T_i}(\phi_T) = \frac{-\tan\Theta_{T_i}}{\sin\beta_{T_i}(\phi_T) + \cos\beta_{T_i}(\phi_T)\tan\Theta_{T_i}}, \quad (26)$$

where $\alpha_{T_i}(\phi_T) > 0$. The modulo operation in Eq. (24) is removed by the tangent function.

According to Eq. (19), the tag gain ratio of G_{T_1} to G_{T_2} can be computed by

$$\frac{G_{T_1}(\phi_T)}{G_{T_2}(\phi_T)} = \sqrt{\frac{d_{T_2}(d_{T_2}+D)}{d_{T_1}(d_{T_1}+D)} \frac{\alpha_{T_2}(\phi_T)}{\alpha_{T_1}(\phi_T)}} \approx \frac{d_{T_2}}{d_{T_1}} \sqrt{\frac{\alpha_{T_2}(\phi_T)}{\alpha_{T_1}(\phi_T)}}, \quad (27)$$

where we assume $(d_{T_i} + D) \approx d_{T_i}$ due to $D \ll d_{T_1}, d_{T_2}$.

2) Coupling RSSI Ratio $\frac{\Gamma_{T_1}(\phi_T)}{\Gamma_{T_2}(\phi_T)}$. We then substitute $\alpha_{T_i}(\phi_T)$ and $\beta_{T_i}(\phi_T)$ into Eq. (16a) to compute $\Gamma_{T_i}(\phi_T)$,

$$\Gamma_{T_i}(\phi_T) = \sqrt{1 + 2\alpha_{T_i}(\phi_T)\cos\beta_{T_i}(\phi_T) + [\alpha_{T_i}(\phi_T)]^2}. \quad (28)$$

Accordingly, the value of $\frac{\Gamma_{T_1}(\phi_T)}{\Gamma_{T_2}(\phi_T)}$ can be determined.

Experiment Observation. We conduct two types of experiments in a low-multipath scenario to estimate ϕ_T. One is to vary the tag separation D from 2 cm to 7 cm. The type of RFID tags used is the single-dipole Impinj E51 tag. Another is to use other two different tag types, i.e., single-dipole Alien 9640 and dual-dipole Impinj H47 tags, at the 4-cm tag separation. The experiment setup is shown in Fig. 5a. RFID tags are attached on a cardboard. We follow the procedure in Section V. B to collect RFID fingerprints. The position and direction of tags relative to a reader antenna are different in each measurement.

Fig. 5b shows that the median values of ϕ_T at different tag separations are -0.095 radians, -0.050 radians, -0.123 radians, -0.237 radians, -0.121 radians and -0.168 radians, respectively.

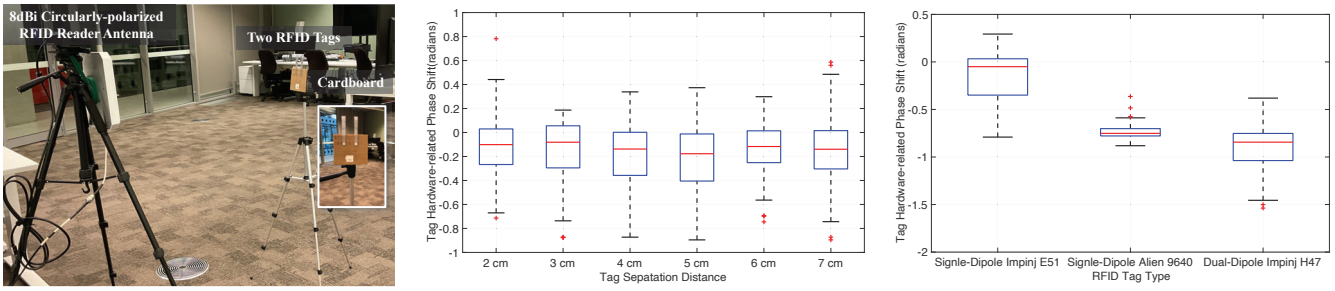

(a) Experiment setup (b) Phase shift over tag separations (c) Phase shift over tag types

Fig. 5: Estimation of tag hardware-related phase shift

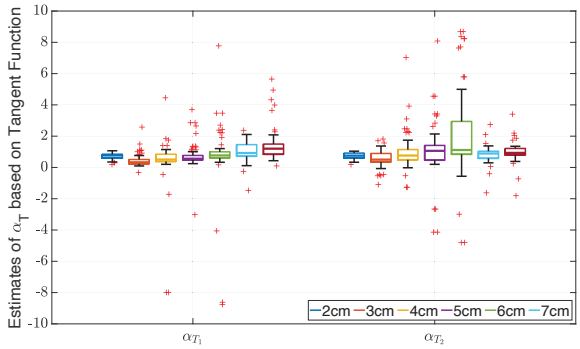

Fig. 6: Estimates of α_{T_1} and α_{T_2} calculated based on Eq. (29).

The results are very close, which is in accordance with our expectation that ϕ_T is a constant term independent of the tag array direction and position relative to the reader antenna. Fig. 5c shows the median values of ϕ_T for different tag types, which are -0.050 radians, -0.751 radians and -0.844 radians. We can see that different tag types may induce different tag hardware-related phase shifts.

D. Estimating tag gain ratio and reflection coefficient

This section aims to verify the impact of tag mutual coupling on tag radiation pattern and reflection coefficient.

Since α_{T_i} in Eq. (19) contains the two parameters of interest, we substitute the estimated ϕ_T^* in the above section into Eq. (26) to calculate $\alpha_{T_1}(\phi_T^*)$ and $\alpha_{T_2}(\phi_T^*)$. However, we find that their estimation accuracy is very sensitive to the phase measurement error since it may be amplified by the tangent function. Instead, we estimate $\alpha_{T_i}(\phi_T^*)$ from Eq. (16b) by

$$\frac{\left[1+\alpha_{T_i}(\phi_T^*)\cos\beta_{T_i}(\phi_T^*)\right]^2}{1+2\alpha_{T_i}(\phi_T^*)\cos\beta_{T_i}+\alpha_{T_i}(\phi_T^*)^2}=(\cos\Theta_{T_i})^2. \quad (29)$$

Unfortunately, there exist two candidates of $\alpha_{T_i}(\phi_T^*)$. To remove the ambiguity, we first calculate $\alpha_{T_i}(\phi_T^*)$ using Eq. (26). The experimental data is from Fig. 5b and the mean value of tag hardware-related phase shifts ϕ_T^* is -0.132 radians. Fig. 6 shows that most of $\alpha_{T_1}(\phi_T^*)$ and $\alpha_{T_2}(\phi_T^*)$ are within the range of $(0, 2]$ at different tag spacings. Thus, we leverage this limitation to obtain the expected $\alpha_{T_i}(\phi_T^*)$.

TABLE I: Scaled reflection coefficient $\epsilon_T G_{T_1,T_2} G_{T_2,T_1}$ over tag spacings estimated by tangent/cosine-based functions

Tag Separation	Tangent-based		Cosine-based	
	Median	Std.	Median	Std.
2 cm	0.717	**0.084**	0.849	**0.129**
3 cm	0.478	**0.333**	0.671	**0.103**
4 cm	0.703	**0.368**	0.707	**0.087**
5 cm	0.792	**0.240**	0.742	**0.097**
6 cm	1.003	**0.614**	0.724	**0.124**
7 cm	0.923	**0.696**	0.837	**0.165**

Based on Eq. (19), the reflection coefficient ϵ_T scaled by $G_{T_1,T_2}G_{T_2,T_1}$ (i.e., $\epsilon_T G_{T_1,T_2}G_{T_2,T_1}$) and the tag gain ratio G_{T_1}/G_{T_2} are estimated by

$$\begin{cases} \epsilon_T G_{T_1,T_2}G_{T_2,T_1} \approx \sqrt{\alpha_{T_1}(\phi_T^*)\alpha_{T_2}(\phi_T^*)}, & (30a) \\ \dfrac{G_{T_1}}{G_{T_2}} \approx \sqrt{\dfrac{\alpha_{T_2}(\phi_T^*)}{\alpha_{T_1}(\phi_T^*)}}\dfrac{d_{T_1}}{d_{T_2}}. & (30b) \end{cases}$$

Experiment Observation. We perform an experiment to observe the variation in the radiation pattern and reflection coefficient in different directions. Fig. 7a plots the experiment setup. A tag array consists of two single-dipole Impinj E51 tags T_1 and T_2 at the 4-cm tag spacing. T_1 is located at the circle center and its distance to a reader antenna is about 80 cm. We vary the direction of a two-tag array by rotating it by an angle increment of $10°$. The reading frequency and transmitted power remain unchanged. We follow Section V. B to collect RFID fingerprints. We have the following findings:

1) Fig. 7b and Fig. 7c show the average RSSI and RF phase of T_1 and T_2 in the non-coupling and coupling cases, respectively. We find that the tag farther from the antenna has a lower RSSI, as if the tag is obstructed by an object.

2) Fig. 8 shows the scaled reflection coefficients in different orientations almost keep unchanged. The average value is 0.724. And we calculate $\epsilon_T G_{T_1,T_2}G_{T_2,T_1}$ under different tag spacings based on the experiment data of Fig. 5b. The results are shown in Table. I. We see that the estimates based on Eq. (29) have a lower standard deviation compared to Eq. (26). The terms ϵ_T, G_{T_1,T_2} and G_{T_2,T_1} are only determined by the tag separation and irrelevant to the array direction.

3) Fig. 9 shows that the tag gain changes with different array angles, which means the mutual coupling effect modifies the radiation pattern of each tag. For comparison, we use the method [33] to simulate the tag radiation pattern of an RFID tag in the absence of tag mutual coupling. Fig. 10a plots it in a

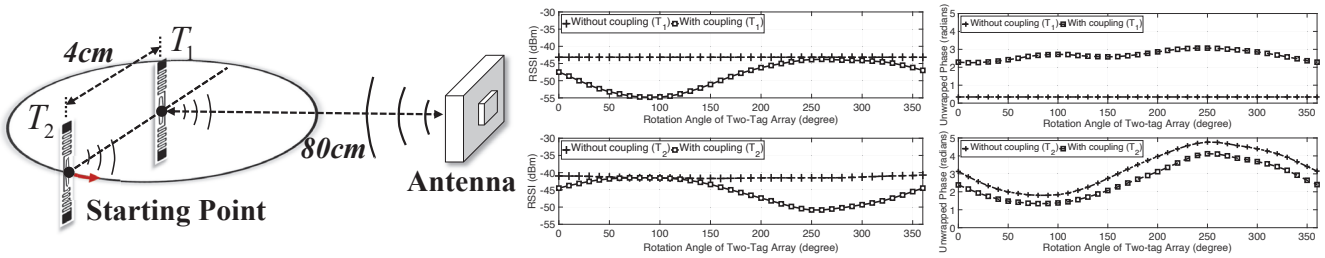

(a) Experiment setup (b) RSSI of T_1 and T_2 (c) Unwrapped RF phase of T_1 and T_2

Fig. 7: Empirical study on tag radiation pattern and reflection coefficient.

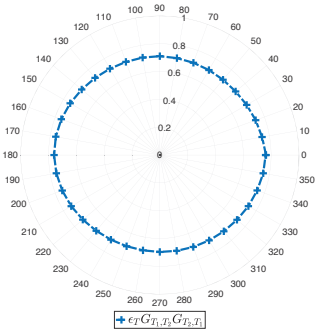

Fig. 8: Scaled reflection coefficient

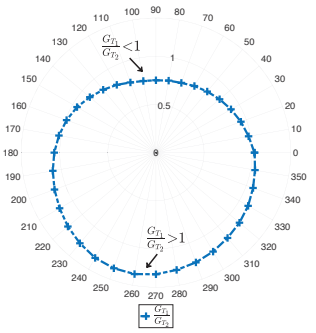

Fig. 9: The ratio of the two tag antenna gains

3-dimensional (3D) space while Fig. 10b and Fig. 10c plot the radiation pattern in the X-Z and Y-Z planes, respectively. We can see that a single-dipole tag radiates equally well in every direction perpendicular to its metal wire and has the same tag gain in the X-Z plane. Accordingly, the ratio of the tag gains in two different directions should be equal to 1, which is different from the case under the mutual coupling effect.

E. Verifying coupling RSSI and coupling phase shift

Here we introduce a method of using a two-RFID-tag array to verify the proposed coupling models. The basic validation idea is to simulate the coupling RSSI Γ_{T_i} or coupling phase shift Θ_{T_i} and then compare the simulated values with the actually-measured ones. To this end, we need to separately simulate two key parameters α_{T_i} and β_{T_i} according to Eq. (16). However, it is very challenging to exactly simulate them since they contain many unknown variables. In this work, we find that since RSSI and RF phase are independent, we can use RF phase measurements in the absence and presence of mutual coupling to derive α_{T_i} and β_{T_i}, and then substitute them into Eq. (16a) to simulate Γ_{T_i}. Similarly, we can use the RSSI measurements in the two cases to obtain α_{T_i} and β_{T_i} and thereby simulate Θ_{T_i} based on Eq. (16b). The detailed simulation processes are described as follows:

We first apply Eq. (20) to calculate β_{T_i}. As described in Section V. B, the RF phase in the non-coupling case are collected and the tag separation D is pre-specified, so we rely on them to calculate the distance difference $(d_{T_1} - d_{T_2})$. Moreover, the tag hardware phase shift ϕ_T is estimated in advance according to Section V.C. We substitute the calculated β_{T_i} into the following simulation.

Verifying coupling RSSI Γ_T using RF phase. *1) Estimated value.* Recall from Eq. (24) that the coupling phase shift Θ_{T_i} can be obtained using the RF phase measurements in the non-coupling and coupling cases. We substitute the estimated Θ_{T_i} and β_{T_i} into Eq. (26) to obtain α_{T_i}. In this case, the coupling RSSI Γ_{T_i} can be simulated using Eq. (16a).

2) Actually-measured value. We divide the measured RSSIs in the coupling and non-coupling cases to obtain

$$\frac{\rho_{T_i}}{\overline{\rho}_{T_i}}\left(\frac{G_{T_i}}{\overline{G}_{T_i}}\right)^2 \Gamma_{T_i} = 10^{\frac{\mathcal{R}^r_{T_i} - \overline{\mathcal{R}}^r_{T_i}}{20}}. \tag{31}$$

Since the tag mutual coupling may not induce significant changes in the modulation factor and tag gain, we assume $\rho_{T_i}/\overline{\rho}_{T_i} \approx 1$ and $G_{T_i}/\overline{G}_{T_i} \approx 1$, so the actually-measured coupling RSSI Γ_{T_i} is

$$\Gamma_{T_i} \approx 10^{\frac{\mathcal{R}^r_{T_i} - \overline{\mathcal{R}}^r_{T_i}}{20}}. \tag{32}$$

Verifying coupling phase shift Θ_T using RSSI. *1) Estimated value.* According to Eq. (32), the coupling RSSI Γ_{T_i} is obtained by using RSSI measurements in the non-coupling and coupling cases, respectively. Then we substitute the calculated Γ_{T_i} and β_{T_i} into Eq. (16a) to obtain α_{T_i}, where $\alpha_{T_i} \in (0, 2]$ as shown in Fig. 6. In this case, we use Eq. (16b) to simulate the coupling phase shift Θ_{T_i}.

2) Actually-measured value. According to Eq. (24), the coupling phase shift Θ_{T_i} can be extracted by using the RF phase measured in the non-coupling and coupling scenarios.

Experiment Observation. Two sets of RFID fingerprints used in Fig. 1 and Fig. 7 are adopted here for coupling term verification. The RFID signal fingerprints are measured in the absence and presence of tag mutual coupling. Fig. 11 shows the corresponding experiment setup. Fig. 12a and Fig. 13a plot the estimated and actually-measured coupling RSSIs Γ_{T_i} in circular and linear-track experiments, while Fig. 10b and Fig. 12b plot the estimated and actually-measured coupling phase shifts Θ_{T_i}. We can see that the estimated Γ_{T_i} and Θ_{T_i} could almost comply with the actual measurements.

F. Verifying tag spacing and tag-antenna distance difference

Based on our proposed models, we combine RSSI and RF phase measurements to derive the tag spacing D and tag-to-antenna distance difference $(d_{T_1} - d_{T_2})$ in the coupling phase shift term. By comparing the estimated values with the actually-measured ones, we can verify our models from another perspective.

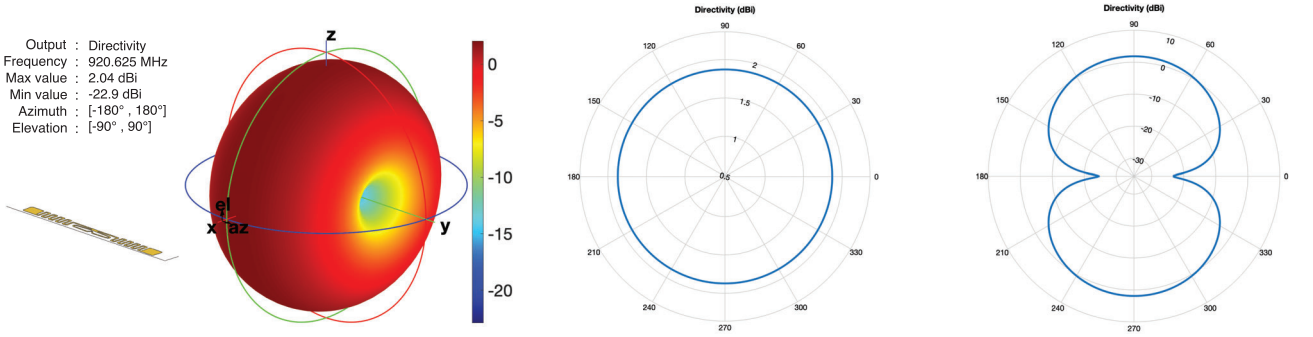

(a) Radiation pattern in 3D space (b) Radiation pattern in the X-Z plane (c) Radiation pattern in the Y-Z plane

Fig. 10: Simulated radiation pattern of a single-dipole Impinj E51 RFID tag in the non-coupling case.

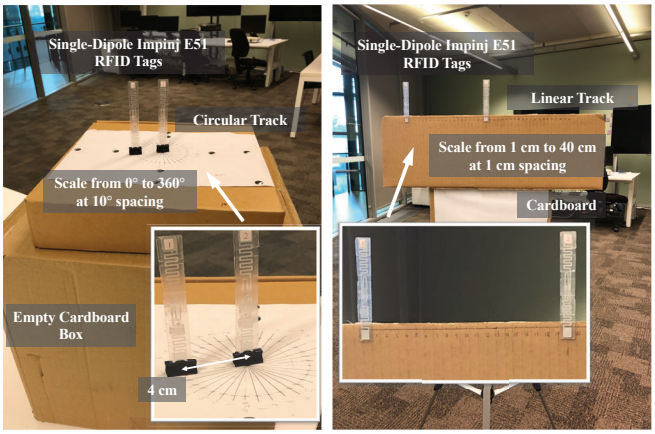

(a) Circular track (b) Linear track

Fig. 11: Experiment setup for coupling model verification.

1) Estimated values. Since Θ_{T_i} and Γ_{T_i} can be calculated using Eq. (24) and Eq. (32), we combine them based on Eq. (16) to obtain

$$\begin{cases} \boldsymbol{U}_{T_i} = \dfrac{\eta_{T_i}\Gamma_{T_i}}{\sqrt{1+(\tan\Theta_{T_i})^2}} - 1 = \alpha_{T_i}\cos\beta_{T_i} \\ \boldsymbol{V}_{T_i} = \dfrac{-\eta_{T_i}\Gamma_{T_i}\tan\Theta_{T_i}}{\sqrt{1+(\tan\Theta_{T_i})^2}} = \alpha_{T_i}\sin\beta_{T_i} \end{cases}, \tag{33}$$

where $\eta_{T_i} = \pm 1$, which is unknown to us. According to the tangent half-angle formula, β_{T_i} can be estimated by

$$\beta_{T_i} = 2\arctan\frac{\boldsymbol{V}_{T_i}}{\sqrt{{\boldsymbol{U}_{T_i}}^2 + {\boldsymbol{V}_{T_i}}^2} + \boldsymbol{U}_{T_i}}. \tag{34}$$

Thus, the tag separation distance and the difference in tag-to-antenna distances are

$$\begin{cases} D = \dfrac{\lambda}{4\pi}\left(\beta_{T_1} + \beta_{T_2} + 2\phi_T + 2\pi k_{T_1,T_2}\right) \\ d_{T_2} - d_{T_1} = \dfrac{\lambda}{4\pi}\left(\beta_{T_1} - \beta_{T_2} + 2\pi\Delta k_{T_1,T_2}\right) \end{cases}, \tag{35}$$

where k_{T_1,T_2} and $\Delta k_{T_1,T_2}$ are unknown integers.

2) Actually-measured values. The tag separation is manually measured using a tape measure. And the tag-to-antenna distance difference between two tags is determined by the RF phases $\overline{\mathcal{P}}_{T_1}$ and $\overline{\mathcal{P}}_{T_2}$ measured in the non-coupling case.

Experiment Observation. The main challenge in the verification experiment is how to determine the unknown term η_{T_i}. In the circular-track experiment, since the mean of $\epsilon_T G_{T_1,T_2} G_{T_2,T_1}$ in Fig. 11a is about 0.7 for the tag spacing of 4 cm and the maximum of G_{T_1}/G_{T_2} in Fig. 11b is about 0.9, the maximum of α_{T_i} is less than 1. To satisfy the requirement for α_{T_i}, we use $\eta_{T_1} = 1$ and $\eta_{T_2} = 1$. In the linear-track experiment, as the tag separation increases, α_{T_i} should be gradually decreasing. We find that when $\eta_{T_1} = 1$ and $\eta_{T_2} = 1$, the change of the estimated α_{T_i} can satisfy this trend. Besides we remove the integers k_{T_1,T_2} and $\Delta k_{T_1,T_2}$ by adding 2π or -2π when 2π-radians of phase ambiguity occurs in the experiments. Fig. 13c and Fig. 13c show that the estimated results could also match well with the actual measurements.

VI. Decoupling for AoA Estimation

This section achieves AoA estimation via decoupling the RFID fingerprints. We first consider an array with two tags, and then study more complicated arrays with more tags.

A. AoA estimation in an array with two tags

In an two-RFID-tag array, the tag elements are the same type and are placed in parallel. According to the model simplification in Section V. A, we remove some unknown polarization terms ($\{\theta_{A,T_1}, \theta_{A,T_2}\}$, $\{\theta_{T_1,T_2}, \theta_{T_2,T_1}\}$, and $\{\mu_{T_1,T_2}, \mu_{T_2,T_1}\}$), so the total CFR $\boldsymbol{H}_{T_1}$ for T_1 can be simplified as

$$\boldsymbol{H}_{T_1} = \rho_{\boldsymbol{H}_{T_1}} e^{-\boldsymbol{J}\phi_{\boldsymbol{H}_{T_1}}}\left(1 + \alpha_{T_1} e^{-\boldsymbol{J}\beta_{T_1}}\right) = 10^{\frac{\mathcal{R}^r_{T_1} - \mathcal{R}^t}{20}} e^{\boldsymbol{J}\left(\mathcal{P}'_{T_1} + \pi k_{T_1}\right)} \tag{36}$$

where

$$\begin{cases} \rho_{\boldsymbol{H}_{T_1}} = \rho_A \rho_T \left(\dfrac{\mu_{A,T_1} G_A G_{T_1}}{d_{T_1}}\right)^2 \\ \phi_{\boldsymbol{H}_{T_1}} = \dfrac{4\pi}{\lambda} d_{T_1} + \phi_A + \phi_T + \pi \\ \alpha_{T_1} = \dfrac{\epsilon_T G_{T_2,T_1} G_{T_1,T_2} G_{T_2}}{G_{T_1}} \dfrac{d_{T_1}}{d_{T_2} + D} \\ \beta_{T_1} = \dfrac{2\pi}{\lambda}\left(d_{T_2} + D - d_{T_1}\right) + \phi_T + \pi \end{cases}. \tag{37}$$

Similarly, we can also obtain the CFR $\boldsymbol{H}_{T_2}$ for T_2. By dividing $\boldsymbol{H}_{T_1}$ by $\boldsymbol{H}_{T_2}$ to eliminate unknown terms (including the RFID reader hardware-related terms (ρ_A and ϕ_A), the

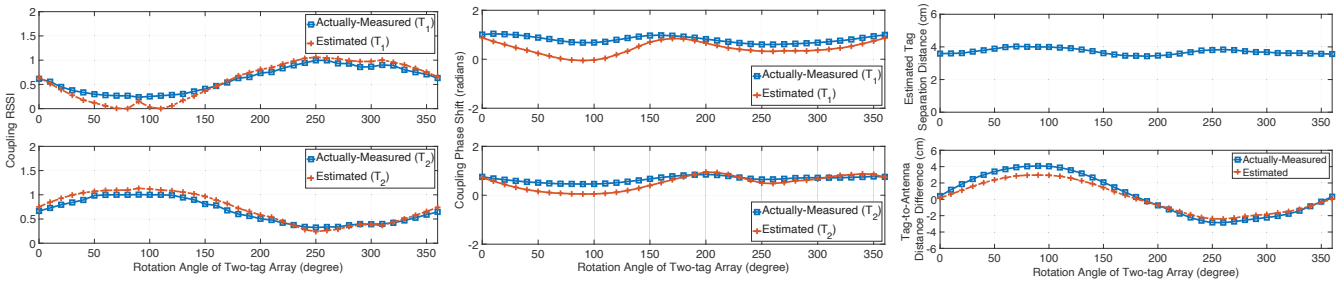

(a) Verifying coupling RSSI using measured RF phase (b) Verifying coupling phase shift using measured RSSI (c) Verifying tag separation and tag-to-antenna distance difference

Fig. 12: Circular-track experiment. The tag T_2 rotates 360° around T_1 and the tag spacing is fixed at 4 cm.

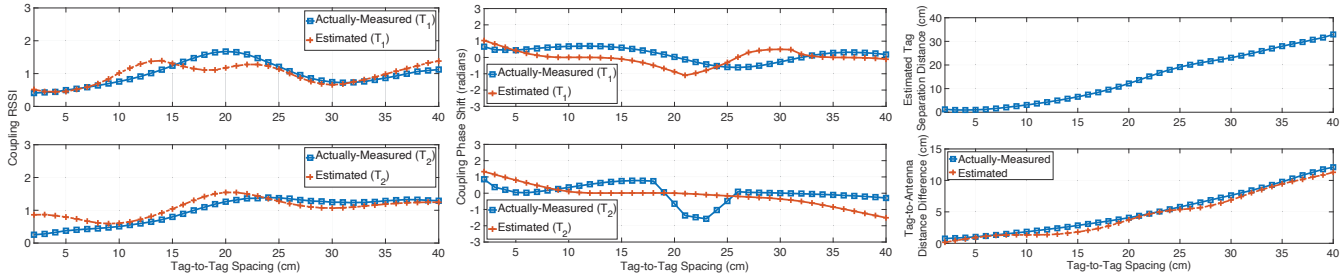

(a) Verifying coupling RSSI using measured RF phase (b) Verifying coupling phase shift using measured RSSI (c) Verifying tag separation and tag-to-antenna distance difference

Fig. 13: Linear-track experiment. The tag T_2 moves away from the fixed tag T_1 and the spacing varies from 2 cm to 40 cm.

reader antenna gain G_A, the modulation factor ρ_T, and the polarization terms $\{\mu_{A,T_1}, \mu_{A,T_2}\}$), we have

$$\frac{\boldsymbol{H}_{T_1}}{\boldsymbol{H}_{T_2}} = \Delta h^{dir}_{T_1,T_2} \frac{1+\Delta h^{ref}_{T_1}}{1+\Delta h^{ref}_{T_2}} = \Delta h_{T_1,T_2}, \tag{38}$$

where

$$\begin{cases} \Delta h^{dir}_{T_1,T_2} = \left(\dfrac{G_{T_1} d_{T_2}}{G_{T_2} d_{T_1}}\right)^2 e^{-\boldsymbol{J}\frac{4\pi}{\lambda}(d_{T_1}-d_{T_2})} \\ \Delta h^{ref}_{T_1} = \dfrac{\epsilon_T G_{T_2,T_1} G_{T_1,T_2} G_{T_2}}{G_{T_1}} \dfrac{d_{T_1}}{d_{T_2}+D} e^{-\boldsymbol{J}\left[\frac{2\pi}{\lambda}(d_{T_2}+D-d_{T_1})+\phi_T+\pi\right]} \\ \Delta h^{ref}_{T_2} = \dfrac{\epsilon_T G_{T_1,T_2} G_{T_2,T_1} G_{T_1}}{G_{T_2}} \dfrac{d_{T_2}}{d_{T_1}+D} e^{-\boldsymbol{J}\left[\frac{2\pi}{\lambda}(d_{T_1}+D-d_{T_2})+\phi_T+\pi\right]} \\ \Delta h_{T_1,T_2} = 10^{\frac{\mathcal{R}^r_{T_1}-\mathcal{R}^r_{T_2}}{20}} e^{\boldsymbol{J}\left[\left(\mathcal{P}'_{T_1}-\mathcal{P}'_{T_2}\right)+\pi\Delta\boldsymbol{k}\right]} \end{cases}. \tag{39}$$

Among them, some variables can be determined as follows:

1) As long as the tag separation and the reading frequency remain unchanged, the tag mutual coupling effect will induce the same impact on the reflection coefficient ϵ_T and the tag gains $G_{T_1,T_2}G_{T_2,T_1}$. Then we can perform a one-time procedure to pre-estimate the scaled reflection coefficient $\epsilon_T G_{T_1,T_2} G_{T_2,T_1}$ using our method in Section V.

2) Since $D \ll d_{T_1}, d_{T_2}$, the values of $d_{T_2}/(d_{T_1}+D)$, $d_{T_2}/(d_{T_1}+D)$, and d_{T_2}/d_{T_1}, are approximately equal to 1.

3) The tag hardware-related phase shift ϕ_T is known to us due to a one-time pre-estimation detailed Section V. C.

4) The integer $\Delta\boldsymbol{k}$ is $\Delta\boldsymbol{k} = k_{T_1} - k_{T_2}$. And the difference between the measured RF phases of T_1 and T_2 is

$$\Delta\Lambda - \pi\Delta\boldsymbol{k} \approx \frac{4\pi}{\lambda}\left(d_{T_1} - d_{T_2}\right), \tag{40}$$

where $\Delta\Lambda = \mathcal{P}'_{T_2} - \mathcal{P}'_{T_1} + \angle\left(\frac{1+\Delta h^{ref}_{T_1}}{1+\Delta h^{ref}_{T_2}}\right)$. If $|d_{T_1} - d_{T_2}| < \lambda/4$, the integer difference $\Delta\boldsymbol{k}$ can be determined by

$$\Delta\boldsymbol{k} = \begin{cases} -2, & \Delta\Lambda \in [-2\pi, -\pi), (d_{T_1} - d_{T_2}) > 0 \\ -1, & \Delta\Lambda \in [-2\pi, -\pi), (d_{T_1} - d_{T_2}) < 0 \\ -1, & \Delta\Lambda \in [-\pi, 0), (d_{T_1} - d_{T_2}) > 0 \\ 0, & \Delta\Lambda \in [-\pi, 0), (d_{T_1} - d_{T_2}) < 0 \\ 0, & \Delta\Lambda \in [0, \pi), (d_{T_1} - d_{T_2}) > 0 \\ 1, & \Delta\Lambda \in [0, \pi), (d_{T_1} - d_{T_2}) < 0 \\ 1, & \Delta\Lambda \in (\pi, 2\pi], (d_{T_1} - d_{T_2}) > 0 \\ 2, & \Delta\Lambda \in (\pi, 2\pi], (d_{T_1} - d_{T_2}) < 0 \end{cases}. \tag{41}$$

Thus, let $\Delta G = G_{T_1}/G_{T_2}$ be the tag gain ratio and θ_{AoA} be the AoA of the backscatter signals received at the tag array, which is calculated by $\theta_{AoA} = \arccos\left[\left(d_{T_1} - d_{T_2}\right)/D\right]$. Based on Eq. (38), the optimal ΔG and θ_{AoA} can be estimated by finding the minimum residual,

$$\underset{\substack{\Delta G\in[0.1,2] \\ \theta_{AoA}\in[-90°,90°]}}{\arg\min} \left\| \Delta h^{dir}_{T_1,T_2}(\Delta G, \theta_{AoA}) \frac{1+\Delta h^{ref}_{T_1}(\Delta G, \theta_{AoA})}{1+\Delta h^{ref}_{T_2}(\Delta G, \theta_{AoA})} - \Delta h_{T_1,T_2} \right\|. \tag{42}$$

where the searching spacings of ΔG and θ_{AoA} are 0.1 and 1° in RF-Mirror. Accordingly, the time complexity is $O(20 \times 181)$. To reduce the computation, we could enlarge the searching spacings of ΔG and θ_{AoA}.

B. AoA estimation in an array with more than two tags

Here we focus on AoA estimation in a tag array consisting of N ($N > 2$) RFID tags, where the spacing between two adjacent tags is less than $\lambda/4$ and the tags are all deployed in parallel. Since each tag may suffer from different mutual coupling interference, its modulation factor and reflection coefficient may be different from others. This makes the AoA

estimation problem more complicated, so the AoA estimation solution on a two-tag array cannot be directly adopted here. Instead, we propose an RFID fingerprint matching solution.

Given two adjacent RFID tags $\boldsymbol{T_j}$ and $\boldsymbol{T_{j+1}}$ in the array, we can make the same assumption like Section VI. A that $d_{\boldsymbol{T_j}}/\left(d_{\boldsymbol{T_j}}+D\right) \approx 1$, $d_{\boldsymbol{T_{j+1}}}/\left(d_{\boldsymbol{T_j}}+D\right) \approx 1$, and $d_{\boldsymbol{T_{j+1}}}/d_{\boldsymbol{T_j}} \approx 1$. On this basis, we divide the CFR $\boldsymbol{H_{T_j}}$ by $\boldsymbol{H_{T_{j+1}}}$ to approximately obtain

$$\frac{\boldsymbol{H_{T_j}}}{\boldsymbol{H_{T_{j+1}}}} = \Delta h^{dir}_{\boldsymbol{T_j},\boldsymbol{T_{j+1}}}\left(\theta_{AoA}\right)\frac{1+\Delta h^{ref}_{\boldsymbol{T_j}}\left(\theta_{AoA}\right)}{1+\Delta h^{ref}_{\boldsymbol{T_{j+1}}}\left(\theta_{AoA}\right)} \approx \Delta h_{\boldsymbol{T_j},\boldsymbol{T_{j+1}}} \tag{43}$$

where

$$\begin{cases} \Delta h^{dir}_{\boldsymbol{T_j},\boldsymbol{T_{j+1}}}\left(\theta_{AoA}\right) \approx \left[\dfrac{\rho_{\boldsymbol{T_j}} G_{\boldsymbol{T_j}}\left(\theta_{AoA}\right)}{\rho_{\boldsymbol{T_{j+1}}} G_{\boldsymbol{T_{j+1}}}\left(\theta_{AoA}\right)}\right]^2 e^{-\boldsymbol{J}\frac{4\pi}{\lambda}D\cos\theta_{AoA}} \\ \Delta h^{ref}_{\boldsymbol{T_j}}\left(\theta_{AoA}\right) \approx \sum\limits_{T_i \neq \boldsymbol{T_j}} \alpha_{\boldsymbol{T_i},\boldsymbol{T_j}}\left(\theta_{AoA}\right) e^{-\boldsymbol{J}\beta_{\boldsymbol{T_i},\boldsymbol{T_j}}\left(\theta_{AoA}\right)} \\ \Delta h^{ref}_{\boldsymbol{T_{j+1}}}\left(\theta_{AoA}\right) \approx \sum\limits_{T_i \neq \boldsymbol{T_{j+1}}} \alpha_{\boldsymbol{T_i},\boldsymbol{T_{j+1}}}\left(\theta_{AoA}\right) e^{-\boldsymbol{J}\beta_{\boldsymbol{T_i},\boldsymbol{T_{j+1}}}\left(\theta_{AoA}\right)} \\ \Delta h_{\boldsymbol{T_j},\boldsymbol{T_{j+1}}} = 10^{\frac{\mathcal{R}^r_{\boldsymbol{T_j}}-\mathcal{R}^r_{\boldsymbol{T_{j+1}}}}{20}} e^{\boldsymbol{J}\left[\left(\mathcal{P}^{'}_{\boldsymbol{T_j}}-\mathcal{P}^{'}_{\boldsymbol{T_{j+1}}}\right)+\pi\Delta\boldsymbol{k}_{\boldsymbol{T_j},\boldsymbol{T_{j+1}}}\right]} \end{cases} \tag{44}$$

And the RF phase $\mathcal{P}^{'}_{\boldsymbol{T_j}}$(or $\mathcal{P}^{'}_{\boldsymbol{T_{j+1}}}$) is the version with the π-phase periodicity. $\Delta\boldsymbol{k}_{\boldsymbol{T_j},\boldsymbol{T_{j+1}}}$ is an unknown integer. Its impact on AoA estimation can be eliminated as follows.

From the above equations, we find that *the tag mutual coupling effect is highly dependent on the tag separation and the orientation of a tag array relative to a reader antenna, rather than the distance between the tag array and the antenna*. Based on this idea, we achieve decoupling for multiple-tag-array AoA estimation using the prior knowledge of RFID fingerprints of all tags in each pre-defined AoA. This is a one-time collection when the tag array is built. For the RFID tag array with more than two tag elements, we assume that $\left\{\widehat{\mathcal{R}}^r_{T_1}\left(\theta_{AoA}\right),\cdots,\widehat{\mathcal{R}}^r_{T_N}\left(\theta_{AoA}\right)\right\}$ and $\left\{\widehat{\mathcal{P}}^{'}_{T_1}\left(\theta_{AoA}\right),\cdots,\widehat{\mathcal{P}}^{'}_{T_N}\left(\theta_{AoA}\right)\right\}$ are the pre-collected RSSI and RF phase measurements in a pre-specified direction θ_{AoA}. We also assume that $\left\{\mathcal{R}^r_{T_1},\cdots,\mathcal{R}^r_{T_N}\right\}$ and $\left\{\mathcal{P}^{'}_{T_1},\cdots,\mathcal{P}^{'}_{T_N}\right\}$ are the RSSI and RF phase measurements of all tag elements in the same tag array that are used to achieve AoA estimation in a practical application. In this case, RF-Mirror can compare them with the prior knowledge of RFID fingerprints in different directions to obtain an optimal AoA. Mathematically, this matching method is achieved as follows:

$$\underset{\theta_{AoA}\in[-90^\circ,90^\circ]}{\arg\min}\sum_{j=1}^{N-1}\left\|\Delta\widehat{h}_{\boldsymbol{T_j},\boldsymbol{T_{j+1}}}\left(\theta_{AoA}\right)-\Delta h_{\boldsymbol{T_j},\boldsymbol{T_{j+1}}}\right\|, \tag{45}$$

where

$$\begin{cases} \Delta\widehat{h}_{\boldsymbol{T_j},\boldsymbol{T_{j+1}}}\left(\theta_{AoA}\right) = 10^{\frac{\widehat{\mathcal{R}}^r_{\boldsymbol{T_j}}\left(\theta_{AoA}\right)-\widehat{\mathcal{R}}^r_{\boldsymbol{T_{j+1}}}\left(\theta_{AoA}\right)}{20}} e^{\boldsymbol{J}\left|\cos\left[\widehat{\mathcal{P}}^{'}_{\boldsymbol{T_j}}\left(\theta_{AoA}\right)-\widehat{\mathcal{P}}^{'}_{\boldsymbol{T_{j+1}}}\left(\theta_{AoA}\right)\right]\right|} \\ \Delta h_{\boldsymbol{T_j},\boldsymbol{T_{j+1}}} = 10^{\frac{\mathcal{R}^r_{\boldsymbol{T_j}}-\mathcal{R}^r_{\boldsymbol{T_{j+1}}}}{20}} e^{\boldsymbol{J}\left|\cos\left(\mathcal{P}^{'}_{\boldsymbol{T_j}}-\mathcal{P}^{'}_{\boldsymbol{T_{j+1}}}\right)\right|} \end{cases} \tag{46}$$

Specifically, we use the absolute value of the cosine function (i.e., $|\cos(\cdot)|$) to remove the impact of the unknown integer $\Delta\boldsymbol{k}_{\boldsymbol{T_j},\boldsymbol{T_{j+1}}}$. When the estimated AoA matches the ground truth, the sum function will have the minimum value.

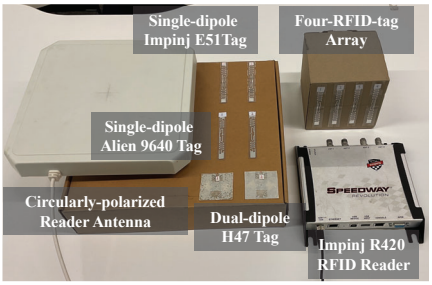

(a) RFID devices and multi-tag array

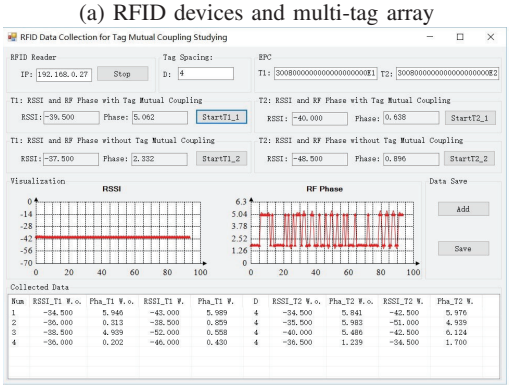

(b) RFID fingerprint collection

Fig. 14: RF-Mirror implementation and software interface

Otherwise, the summation value will become larger. Such a searching complexity is $O(M)$, where M is the number of pre-defined angles for prior measurement. However, it is a time-consuming process to pre-collect RFID fingerprints in all spatial directions. In RF-Mirror, we only deploy the center points of an antenna and RFID tags in the same plane. Following the experiment setup in Fig. 7a, we rotate the tag array around the circle center by 360° at a 10° angular interval.

VII. Implementation & Evaluation

Hardware and Software. We test RF-Mirror using an Impinj R420 RFID reader, an E9208PCRNF antenna with 8 dBi gain and circular polarization, single-dipole Impinj E51 tags, single-dipole Alien 9640 tags and dual-dipole Impinj H47 RFID tags, shown in Fig. 14a. The reader is set in the Miller-encoding reader mode of 'Dense Reader M4' (which induces the π-radians phase jump), the search mode of Dual Target Session 0, the transmitted power of 32 dBm and the operating frequency of 920.625 MHz. We exploit the Impinj Octane SDK [34] to develop an RFID fingerprint collection program in C#, which can record an RFID tags's electronic product code, RSSI and RF phase, shown in Fig. 14b.

Default Experiment Setup. The RFID tag type is single-dipole Impinj E51; the separation distance between two adjacent tags is 4 cm (less than a quarter of wavelength); all tags are placed in parallel and form a linear uniform array. Besides, a multi-tag array used in this work consists of four RFID tags and is attached to a cardboard box.

Experimental scenarios. As shown in Fig. 15, we evaluate RF-Mirror's performance in low-multipath LOS, low-multipath NLOS and rich-multipath LOS scenarios, respectively. In a low-multipath LOS scenario, objects are far away

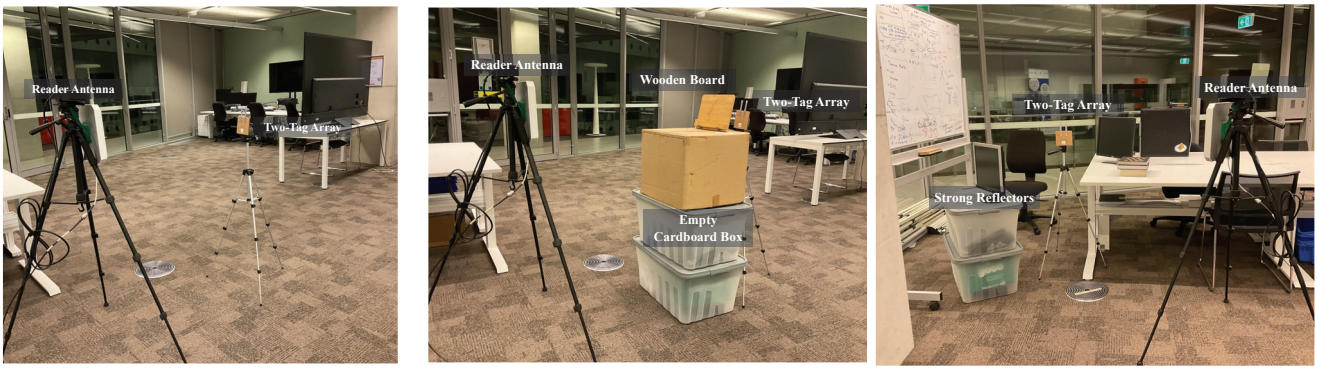

(a) Low-multipath LOS (b) Low-multipath NLOS (c) Rich-multipath LOS

Fig. 15: Experiment scenarios

from our RFID tag array and no obstacles block the direct propagation path between a reader antenna and the array. In a NLOS scenario, we block the tag-to-antenna LOS path using a wooden board. In a rich-multipath scenario, we randomly place hardcover books, computer monitors and chairs around the tags, together with a person walking around but without blocking the LOS path.

Methodology. We randomly change the direction and distance of our tag array relative to a reader antenna in 3D space each time. In the two-tag-array experiment, we need to pre-estimate a scaled reflection coefficient using the method described in Section V. In the four-tag-array experiment, the prior knowledge is collected in a 2D plane (RFID tags and a reader antenna center are in the same plane). However, we still adjust the height of a reader antenna to collect the 3D-space data for evaluation.

Baselines. Most existing systems configure an RFID reader in the FM0-encoding reader mode of 'Max Throughput'. The reported RF phase only has the 2π-radians phase periodicity, which can be easily eliminated. Two baselines are adopted in this mode for comparison: *1)* A commonly-used AoA estimation method (called *Phase-difference*), which directly calculates PDoA between adjacent RFID tags to estimate an object's AoA without considering any impact of tag mutual coupling [3], [5], [6], [31], and *2)* the Tagyro [2] method, which deals with the coupling impact by pre-estimating a virtual tag separation to replace the actual one. *Recall that in our RF-Mirror scheme, the tags are configured in the more practical 'Dense Reader M4' mode with Miller-encoding and potentially stronger RF noise tolerance, but facing the problem of π-radians phase jump.*

Metric and Ground Truth. To characterize RF-Mirror's performance, we define the AoA estimation error, i.e., the deviation of the estimated AoA from the ground truth. The ground-truth AoA is obtained based on Eq. (1) and Eq. (3) by measuring each tag's RF phase in a non-coupling and low-multipath scenario, where we manually specify which tag is closer to the reader antenna. In the four-tag-array experiment, we collect the RF phases of two tags in the non-coupling case to measure the ground-truth AoA. In addition, in low-multipath NLOS and rich-multipath LOS scenarios, we firstly obtain the ground truth and then use obstacles or other objects to build the corresponding scenario for evaluation.

VIII. Results

This section evaluates the AoA estimation performance of RF-Mirror in two- and four-tag arrays.

A. Comparison to state-of-the-art

We start by comparing our scheme with the baselines in a two-tag array. For fairness, the experiment is conducted in a low-multipath LOS scenario so that we can ignore the impact of multipath interference. The experiment is repeated more than 100 times. For Tagyro, we first rotate the two-tag array by 360° and find the the maximum PDoA to estimate an *effective tag separation*. According to the experiment in Fig. 10a, the *effective tag separation* is 3.2 cm while the ground truth is 4 cm. We also use other virtual tag spacings of 2 cm, 5 cm and 8 cm in Tagyro for evaluation. Fig. 16 shows that the median AoA error of RF-Mirror is 11.65°, significantly outperforming Phase-Difference, Tagyro-2cm, Tagyro-3.2cm, Tagyro-5cm and Tagyro-8cm by 5.49 times, 5.92 times, 5.96 times, 5.06 times and 2.63 times, respectively. Moreover, the 80-percentile and 90-percentile AoA errors of RF-Mirror are less than 30.36° and 40.15° for the two-tag array. The comparison of AoA estimation accuracy is shown in Table II. Since the tag mutual coupling effect may induce random changes in RF phase on each tag, the Phase-Difference method cannot cancel the RF phase distortion. The Tagyro method may not always work well. According to our proposed models, the coupling phase shift varies with different tag-antenna directions (dependent on the tag radiation pattern), so it is challenging to calibrate using the constant *effective tag spacing* for making Tagyro work effective in practice. Besides, since the impact of the 2π-radians phase periodicity cannot be corrected, the methods of Phase-Difference and Tagyro may result in the larger AoA error.

B. AoA measurement accuracy in different multipath scenarios

In this experiment, we evaluate the AoA accuracy of the two-tag and four-tag arrays in low-multipath LOS, low-multipath NLOS, rich-multipath LOS scenarios, respectively. We first collect RFID fingerprints in a low-multipath LOS

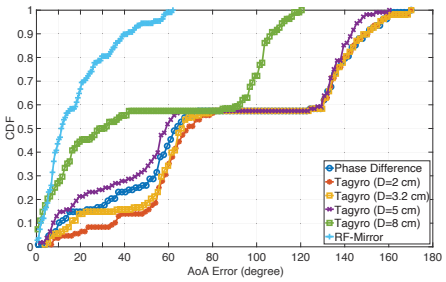

Fig. 16: AoA error of RF-Mirror compared to Phase Difference and Tagyro

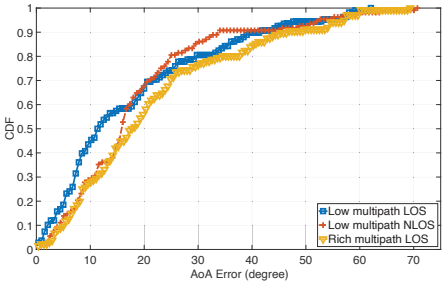

Fig. 17: AoA error of two-tag array under different scenarios

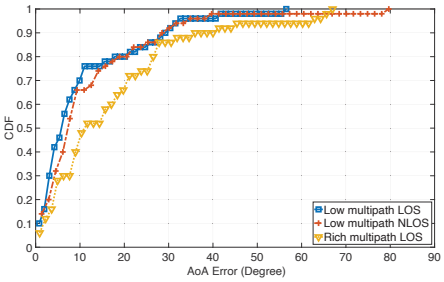

Fig. 18: AoA error of four-tag array under different scenarios

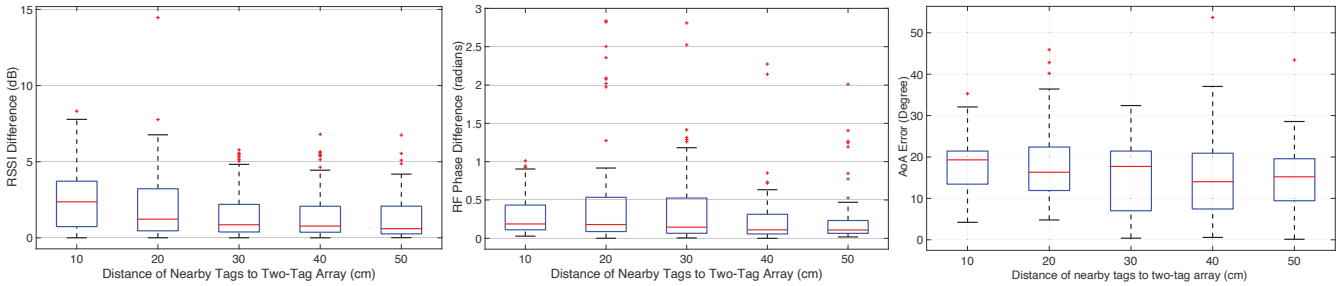

(a) The variation in RSSI (b) The variation in RF phase (c) AoA error

Fig. 19: Impact of the distance of other nearby RFID tags to the two-tag array

TABLE II: AoA accuracy comparison

Method	50^{th} percentil (degrees)	80^{th} percentil (degrees)	90^{th} percentil (degrees)
Phase-Difference	64.1°	141.7°	149.6°
Tagro (D=2 cm)	69.4°	139.7°	150.4°
Tagro (D=3.2 cm)	66.0°	140.7°	148.4°
Tagro (D=5 cm)	59.5°	138.0°	144.1°
Tagro (D=8 cm)	29.7°	102.5°	107.6°
RF-Mirror (Ours)	**11.65°**	**30.36°**	**40.15°**

scenario and then keep the positions of RFID tags unchanged and set up low-multipath NLOS and rich-multipath LOS environment. Fig. 17 shows that the median AoA errors of the two-tag array in the three cases are 11.34°, 16.05° and 18.25°. The 80-percentile AoA errors are 25.05°, 29.78° and 37.67°. Fig. 18 shows that the median AoA errors of the four-tag array are 6.28°, 8.13° and 11.58°. And the 80-percentile AoA errors are 17.87°, 18.92° and 26.53°. From the results, we have the following findings:

1) As expected, the AoA errors in the low-multipath NLOS and rich-multipath LOS scenarios are slightly higher than the error in the low-multipath LOS. In a low-multipath NLOS case, RF signals penetrate the wooden board twice back to an antenna receiver, thereby degrading the signal-to-noise ratio (SNR) compared to the LOS case. The impact of environmental noise thus becomes severe. Also, the reflections from the wooden board may introduce additional phase shifts on each tag and impact the AoA accuracy. In a rich-multipath LOS case, the performance degradation is insignificant. We find that tag mutual coupling may sometimes improve each tag's SNR in some directions. The higher SNR may effectively suppress multipath interference.

2) More RFID tags can lead to higher AoA accuracy. Such a result is also expected since more tags provide more orientation-dependent RFID fingerprints. Specifically, the prior knowledge of RFID fingerprints and the corresponding AoA is collected in a 2D plane while the test data in practical applications is measured in 3D space. The tag gains in different spatial directions are a little different from those in a 2D plane. If more prior knowledge is provided, the AoA accuracy in the four-tag array could be further improved.

C. AoA estimation accuracy vs. different parameters

Next, we evaluate RF-Mirror performance in a two-tag array under five different experiment settings, including nearby RFID tags, tag separation distance, tag-to-antenna distance, tag array deployment and tag type.

Impact of nearby RFID tags. We first measure the RFID fingerprint of each tag when no other tags are around the array. To observe the changes in the RSSI and RF phase of the two tags, we randomly place eight tags around them. Then we compute the RSSI and RF phase differences before and after placing these nearby tags. The distances of these nearby tags to the tag array range from 10 cm to 50 cm at about 10 cm spacing. The positions of the tags in the array remain unchanged in each experiment.

Fig. 19a shows that the median of RSSI difference decreases from 2.365 dB to 0.605 dB as these nearby tags locate gradually away from the two-tag array. Fig. 19b shows that the median of RF phase difference reduces from 0.187 radians to 0.109 radians. The nearby tags result in the variation of the RFID fingerprint. Since the impact of tag mutual coupling is inversely proportional to the separation distance between tags, the differences decrease with distance increasing. This can be seen clearly from Fig. 19c.

Impact of tag separation distance. To evaluate the impact of different tag spacings on the AoA accuracy, we apply the pre-estimated reflection coefficients (see Table. I) into our

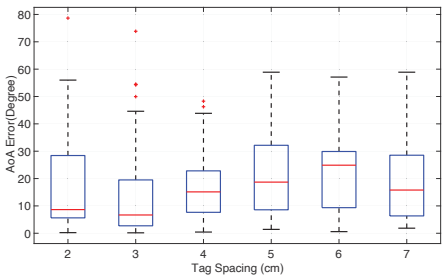

Fig. 20: Impact of tag separation

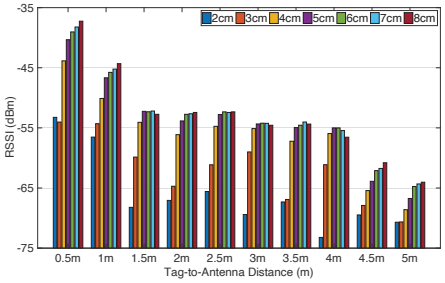

Fig. 21: RSSI over tag separation distance

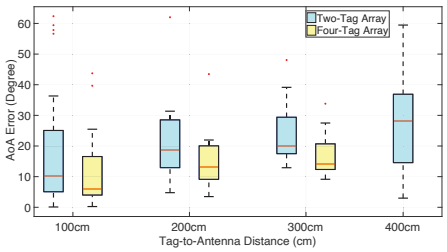

Fig. 22: Impact of tag-antenna distance

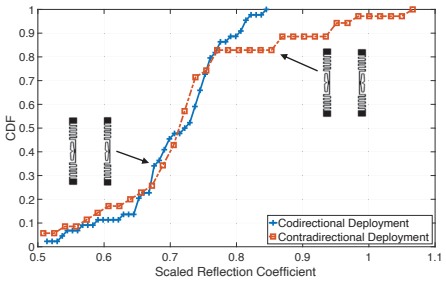

Fig. 23: Scaled reflection coefficients

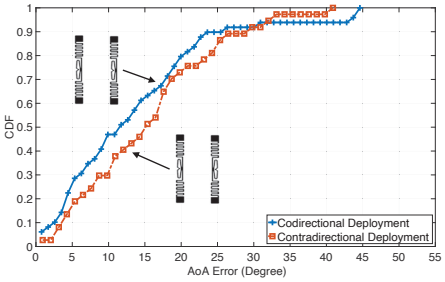

Fig. 24: Robustness to array deployment

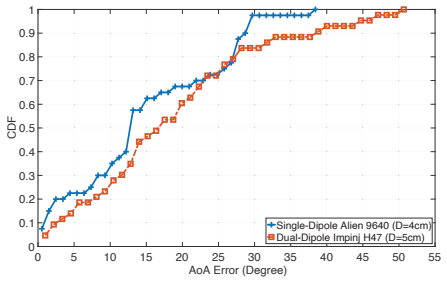

Fig. 25: Impact of RFID tag type

model for evaluation. Fig. 20 shows that the AoA error slightly increases as the tag spacing increases. Although the larger tag spacing should strengthen the tolerance to the measurement error in RF phase, we cannot ignore the impact of multipath interference in practical environments. According to [35], the larger the tag spacing is, the more different the multipath impact on each tag will be. It means the calculated PDoA for AoA estimation may contain more noise, thereby reducing the AoA accuracy.

In the experiment, we also find that a smaller tag spacing may produce a more serious shielding effect. The shadowed RFID tag (farther from a reader antenna) in a two-tag array may require higher power to be activated. Here we conduct an experiment to illustrate this effect by deploying the centers of a reader antenna and two tags in a straight line. A tag (e.g., T_1) is located between the antenna and another tag (e.g., T_2). The shadowed tag is T_2. We vary the position of the tag T1 to adjust the tag spacing from 2 cm to 8 cm. Also, we vary the distance of the tag array to the antenna from 50 cm to 500 cm. Fig. 21 shows that the RSSI of T_2 at a smaller tag spacing is much lower than that at a larger tag spacing. Recall from Fig. 1c that even a 8-cm tag spacing still leads to a severe change in the RF phase due to the tag mutual effect. In this case, we suggest using $4cm \sim 6cm$ tag spacing which is appropriate for balancing the shielding effect and the AoA estimation accuracy in practical applications.

Impact of tag-to-antenna distance. We vary the tag-to-antenna from 100 cm to 400 cm at 100 cm spacing. Here we also test its impact on the four-tag-array system. Specifically, the prior knowledge for our matching method is the same under the different tag-to-antenna distances. As shown in Fig. 22, the median AoA errors for the two-tag array are $10.21°$, $18.66°$, $20.04°$ and $28.05°$, while those for the four-tag array are $6.04°$, $13.26°$ and $14.14°$. The experiment result shows that the AoA error increases gradually as the tag-to-antenna distance increases. As the distance increases, the transmitted signal power arriving at the tag end for backscatter signal modulation will accordingly decrease. Due to the reduced SNR, the impact of environmental noise will be strengthened, resulting in an increase in the AoA error. When the tags are relatively far from the reader antenna, the shadowed RFID tag may not be read in some directions. To deal with this issue, we should increase the tag separation distance in long-range applications.

Robustness to RFID tag array deployment. In this experiment, we test the robustness of RF-Mirror to different array deployments. Different tag array deployments can excite different electromagnetic distributions on each tag and result in different radiation patterns. Fig. 23 shows that the scaled reflection coefficients of the co-directional and contra-directional tag deployments are 0.728 and 0.725, which are very close to the value in our default deployment (i.e., 0.703). We then apply our proposed RF-Mirror scheme to estimate the AoA for these deployments. Fig. 24 shows the median AoA errors are $11.88°$ and $15.55°$ for these two different deployments, which are close to $11.65°$ in our default deployment. This demonstrates that RF-Mirror is robust to array deployment.

Robustness to RFID tag type. Here we use single-dipole Alien 9640 and dual-dipole Impinj H47 RFID tags to study on the impact of different tag types. A dual-dipole tag is equipped with two orthogonal dipole antennas and can achieve an approximately isotropic radiation pattern. Since the size of a H47 RFID tag is about $4.4cm \times 4.4cm$, the tag separation is set to 5 cm here. We firstly collect some data to estimate the scaled reflection coefficients of Alien 9640 and Impinj H47 RFID tags (0.884 and 1.067, respectively). The pre-estimated tag hardware-related phase shifts are -0.751 radians and -0.844 radians, as shown in Fig. 7c. These constants are then used in estimating the AoA. Fig. 25 shows that the median AoA errors are $13.11°$ and $17.17°$. The 80-percentile AoA errors

of the two-tag array are $26.77°$ and $27.01°$. We can see that RF-Mirror also works well for other types of tag arrays.

IX. Related Work

In this section, we review the state-of-the-art literature most closely related to our work.

Single Tag-based Localization. Each object to be tracked is attached with an RFID tag. To combat 2π RF phase periodicity, some localization approaches like RF-IDraw [17] and BackPos [29] require deploying multiple reader antennas around the region of interest and putting a strict constraint on two adjacent antennas' spacing. Some motion-based localization approaches like Tagoram [20], MobiTagbot [36], RFly [37], RF-Scanner [38], AdaRF [21] and RF-3DScan [39] require moving a reader antenna or an RFID tag carried by a robot or drone with a predefined track or trajectory. Recently, some RFID and computer vision fusion methods are proposed. RF-MVO [40] can deal with unpredictable trajectory cases by attaching a light-weight 2D monocular camera on reader antennas. TaggedAR [41], TagVision [42], and RF-Focus [35] use a camera to extract image regions of containing objects, and then match them with each RFID tag by fusing RF phase measurements and the distance captured by the camera. RFind [43] performs by measuring time-of-flight from an RFID tag to each reader antenna, which could effectively deal with multipath interference. However, RFind requires a customized hardware to transmit and receive specified RF signals through a tag, and needs to take a few seconds for frequency hopping. Accurately tracking a moving RFID tag is challenging.

Multiple Tag-based Localization & Sensing. *1) Device-based Solutions.* Each target object is attached with multiple tags. RF-Dial [6], RF-Kinect [44], and One-more-tag [3] use PDoA between tag elements for position or orientation tracking. Spin-Antenna [13] leverages array-antenna polarization mismatch to track tagged object movement. And many works are designed based on the changes in RSSI and RF phase of tag elements in the tag array for fingertip identification [10], position-independent authentication [45], sound vibration sensing [46], heart rate assessment [47], and wearable body-frame tracking [48]. *2) Device-free Solutions.* Each target is tracked without carrying any RFID tags. RFID tags in a tag array are regarded as virtual receiving antennas. Tadar [49], RF-HMS [50], RFIPad [51], and GRfid [52] receive the reflections from human body and hands for position and gesture recognition. TagScan [53] is proposed for target imaging by determining whether the direct path between the tag array and reader antenna is blocked. For above multi-tag systems, their sensing accuracy suffers from mutual coupling interference among RFID tags. The proposed RF-Mirror aims to minimize its impact and obtain more accurate RSSI and RF phase for sensing use.

Mutual Coupling-based RFID Localization & Orientation Tracking. Twins [9], Trio [32], and SparseTag [54] leverage tag mutual coupling for object tracking. When two RFID tags are tightly spaced, tag mutual coupling may induce the obvious differences in RSSI or RF phase. By determining the absence or presence of tag mutual coupling, they could achieve coarse-resolution position estimation. However, these works require pre-deploying many reference RFID tags in regions of interest. In [1], the authors achieve the AoA estimation on a two-tag array by pre-collecting the prior knowledge of RFID fingerprints in pre-defined directions. However, this work designs a novel AoA searching method for a two-tag array without providing any prior knowledge. Also, we extend the decoupling method to achieve AoA estimation on an array with more than two tags.

Tag Radiation Pattern. Pattern multiplication theorem [55] is used to model the radiation pattern of a tag array. However, it requires that each antenna is uncoupled, which cannot be applied in this work. Some works [56], [57] indicate that tag mutual coupling may affect the reading performance of stacked RFID tags. However, they need specialized devices to measure mutual impedances between tags for analyzing. Feng et al. [58] demonstrate that tag mutual coupling can enhance the tag gain in some tag-to-antenna directions while weaken the gain in others. However, its RFID signal models ignore the variation in the modulation factor of each tag element due to the mutual coupling effect. Stefano et al. [59] design a two-tag array system for building crack monitoring based on the fact that mutual impedance is sensitive to the change in the tag-to-tag spacing. However, the work is unable to calculate the tag radiation pattern. In our system, we visualize the change in the tag radiation pattern by calculating the tag gain ratio.

X. Conclusion

We present RF-Mirror, a scheme that enables compensating the distortions in RSSI and RF phase caused by the tag mutual coupling effect in an RFID tag array, to achieve fine-grained AoA estimation. In this paper, novel RSSI and RF phase-distance models are developed to characterize the coupling effect. A series of model validation experiments are conducted, with the application of specifically developed signal processing techniques. These experimental results verify the effectiveness of the proposed models. Using the validated new models, AoA estimation algorithms are developed for RFID arrays with two and more than two tags, respectively. Our RF-Mirror scheme has been tested thoroughly using COTS RFID devices, with extensive experimental results reported in the paper. The experimental results demonstrate that RF-Mirror can achieve significantly improved AoA estimation accuracy in multi-tag RFID arrays compared to prior methods.

References

[1] Z. Wang, M. Xu, N. Ye, H. Huang, R. Wang, and F. Xiao, "Rf-mirror: Mitigating mutual coupling interference in two-tag array labeled rfid systems," in *IEEE SECON*, 2020, pp. 1–9.

[2] T. Wei and X. Zhang, "Gyro in the air: tracking 3d orientation of batteryless internet-of-things," in *ACM MobiCom*, 2016, pp. 55–68.

[3] F. Xiao, Z. Wang, N. Ye, R. Wang, and X.-Y. Li, "One more tag enables fine-grained rfid localization and tracking," *IEEE/ACM Transactions on Networking*, vol. 26, no. 1, pp. 161–174, 2018.

[4] J. Guo, T. Wang, Y. He, M. Jin, C. Jiang, and Y. Liu, "Twinleak: Rfid-based liquid leakage detection in industrial environments," in *IEEE INFOCOM*, 2019, pp. 883–891.

[5] Y. Bu, L. Xie, Y. Gong, J. Liu, B. He, J. Cao, B. Ye, and S. Lu, "Rf-3dscan: Rfid-based 3d reconstruction on tagged packages," *IEEE Transactions on Mobile Computing*, vol. 20, no. 2, pp. 722–738, 2019.

[6] Y. Bu, L. Xie, Y. Gong, C. Wang, L. Yang, J. Liu, and S. Lu, "Rf-dial: Rigid motion tracking and touch gesture detection for interaction via rfid tags," *IEEE Transactions on Mobile Computing*, 2020.

[7] J. Ning, L. Xie, C. Wang, Y. Bu, F. Xu, D.-W. Zhou, S. Lu, and B. Ye, "Rf-badge: Vital sign-based authentication via rfid tag array on badges," *IEEE Transactions on Mobile Computing*, 2021.

[8] W. Xu, J. Liu, S. Zhang, Y. Zheng, F. Lin, J. Han, F. Xiao, and K. Ren, "Rface: anti-spoofing facial authentication using cots rfid," in *IEEE INFOCOM 2021-IEEE Conference on Computer Communications*. IEEE, 2021, pp. 1–10.

[9] J. Han, C. Qian, X. Wang, D. Ma, J. Zhao, W. Xi, Z. Jiang, and Z. Wang, "Twins: Device-free object tracking using passive tags," *IEEE/ACM Transactions on Networking*, vol. 24, no. 3, pp. 1605–1617, 2016.

[10] C. Zhao, Z. Li, T. Liu, H. Ding, J. Han, W. Xi, and R. Gui, "Rf-mehndi: A fingertip profiled rf identifier," in *IEEE INFOCOM*, 2019, pp. 1513–1521.

[11] G. Wang, H. Cai, C. Qian, J. Han, S. Shi, X. Li, H. Ding, W. Xi, and J. Zhao, "Hu-fu: Replay-resilient rfid authentication," *IEEE/ACM Transactions on Networking*, vol. 28, no. 2, pp. 547–560, 2020.

[12] D. Xie, D. Weidman, S. Yao, A. Tang, and X. Wang, "3d passive positioning based on rfid tag array," in *ICC 2019-2019 IEEE International Conference on Communications (ICC)*. IEEE, 2019, pp. 1–6.

[13] C. Wang, L. Xie, K. Zhang, W. Wang, Y. Bu, and S. Lu, "Spin-antenna: 3d motion tracking for tag array labeled objects via spinning antenna," in *IEEE INFOCOM*, 2019, pp. 1–9.

[14] C. Yang, X. Wang, and S. Mao, "Rfid tag localization with a sparse tag array," *IEEE Internet of Things Journal*, 2021.

[15] Z. Chen, P. Yang, J. Xiong, Y. Feng, and X.-Y. Li, "Tagray: Contactless sensing and tracking of mobile objects using cots rfid devices," in *IEEE INFOCOM 2020-IEEE Conference on Computer Communications*. IEEE, 2020, pp. 307–316.

[16] C. Luo, Z. Yang, X. Feng, J. Zhang, H. Jia, J. Li, J. Wu, and W. Hu, "Rfaceid: Towards rfid-based facial recognition," *Proceedings of the ACM on Interactive, Mobile, Wearable and Ubiquitous Technologies*, vol. 5, no. 4, pp. 1–21, 2021.

[17] J. Wang, D. Vasisht, and D. Katabi, "Rf-idraw: virtual touch screen in the air using rf signals," *ACM SIGCOMM Computer Communication Review*, vol. 44, no. 4, pp. 235–246, 2015.

[18] R. Miesen, A. Parr, J. Schleu, and M. Vossiek, "360 carrier phase measurement for uhf rfid local positioning," in *IEEE International Conference on RFID-Technologies and Applications*, 2013, pp. 1–6.

[19] J. Skinner, "Reader modes made easy," https://support.impinj.com/hc/en-us/articles/360000046899-Reader-Modes-Made-Easy, 2020.

[20] L. Yang, Y. Chen, X.-Y. Li, C. Xiao, M. Li, and Y. Liu, "Tagoram: Real-time tracking of mobile rfid tags to high precision using cots devices," in *ACM MobiCom*, 2014, pp. 237–248.

[21] H. Xu, D. Wang, R. Zhao, and Q. Zhang, "Adarf: Adaptive rfid-based indoor localization using deep learning enhanced holography," *ACM IMWUT*, vol. 3, no. 3, pp. 1–22, 2019.

[22] J. Wang, L. Chang, O. Abari, and S. Keshav, "Are rfid sensing systems ready for the real world?" in *ACM Mobisys*, 2019, pp. 366–377.

[23] D. M. Dobkin, *The rf in RFID: uhf RFID in practice*. Newnes, 2012.

[24] A. Boaventura, J. Santos, A. Oliveira, and N. B. Carvalho, "Perfect isolation: Dealing with self-jamming in passive rfid systems," *IEEE Microwave Magazine*, vol. 17, no. 11, pp. 20–39, 2016.

[25] J. D. Griffin and G. D. Durgin, "Complete link budgets for backscatter-radio and rfid systems," *IEEE Antennas and Propagation Magazine*, vol. 51, no. 2, pp. 11–25, 2009.

[26] C. T. A. Johnk, "Engineering electromagnetic fields and waves," *nyjw*, 1975.

[27] J. A. Shaw, "Radiometry and the friis transmission equation," *American journal of physics*, vol. 81, no. 1, pp. 33–37, 2013.

[28] W. L. Stutzman and G. A. Thiele, *Antenna theory and design*. John Wiley & Sons, 2012.

[29] T. Liu, Y. Liu, L. Yang, Y. Guo, and C. Wang, "Backpos: High accuracy backscatter positioning system," *IEEE Transactions on Mobile Computing*, vol. 15, no. 3, pp. 586–598, 2015.

[30] X. Lai, Z. Cai, Z. Xie, and H. Zhu, "A novel displacement and tilt detection method using passive uhf rfid technology," *Sensors*, vol. 18, no. 5, p. 1644, 2018.

[31] C. Jiang, Y. He, X. Zheng, and Y. Liu, "Omnitrack: Orientation-aware rfid tracking with centimeter-level accuracy," *IEEE Transactions on Mobile Computing*, vol. 20, no. 2, pp. 634–646, 2019.

[32] H. Ding, J. Han, C. Qian, F. Xiao, G. Wang, N. Yang, W. Xi, and J. Xiao, "Trio: Utilizing tag interference for refined localization of passive rfid," in *IEEE INFOCOM*, 2018, pp. 828–836.

[33] V. Iyer and A. Taylor, "Antenna model generation and full-wave analysis from a photo," https://au.mathworks.com/help/antenna/examples/antenna-model-generation-and-full-wave-analysis-from-a-photo.html, 2018.

[34] "Octane sdks for .net," https://support.impinj.com/hc/en-us/articles/202755268-Octane-SDK.

[35] Z. Wang, M. Xu, N. Ye, R. Wang, and H. Huang, "Rf-focus: Computer vision-assisted region-of-interest rfid tag recognition and localization in multipath-prevalent environments," *ACM IMWUT*, vol. 3, no. 1, p. 29, 2019.

[36] L. Shangguan and K. Jamieson, "The design and implementation of a mobile rfid tag sorting robot," in *ACM MobiSys*, 2016, pp. 31–42.

[37] Y. Ma, N. Selby, and F. Adib, "Drone relays for battery-free networks," in *ACM SIGCOMM*, 2017, pp. 335–347.

[38] J. Liu, F. Zhu, Y. Wang, X. Wang, Q. Pan, and L. Chen, "Rf-scanner: Shelf scanning with robot-assisted rfid systems," in *IEEE INFOCOM*, 2017, pp. 1–9.

[39] Y. Bu, L. Xie, Y. Gong, J. Liu, B. He, J. Cao, B. Ye, and S. Lu, "Rf-3dscan: Rfid-based 3d reconstruction on tagged packages," *IEEE Transactions on Mobile Computing*, vol. 20, no. 2, pp. 722 – 738, 2021.

[40] Z. Wang, M. Xu, N. Ye, F. Xiao, W. none Ruchuan, and H. Huang, "Computer vision-assisted 3d object localization via cots rfid devices and a monocular camera," *IEEE Transactions on Mobile Computing*, vol. 20, no. 3, pp. 1893 – 908, 2021.

[41] L. Xie, C. Wang, Y. Bu, J. Sun, Q. Cai, J. Wu, and S. Lu, "Taggedar: An rfid-based approach for recognition of multiple tagged objects in augmented reality systems," *IEEE Transactions on Mobile Computing*, vol. 18, no. 5, pp. 1188–1202, 2018.

[42] C. Duan, X. Rao, L. Yang, and Y. Liu, "Fusing rfid and computer vision for fine-grained object tracking," in *IEEE INFOCOM*. IEEE, 2017, pp. 1–9.

[43] Y. Ma, N. Selby, and F. Adib, "Minding the billions: Ultra-wideband localization for deployed rfid tags," in *ACM MobiCom*, 2017, pp. 248–260.

[44] C. Wang, J. Liu, Y. Chen, L. Xie, H. B. Liu, and S. Lu, "Rf-kinect: A wearable rfid-based approach towards 3d body movement tracking," *ACM IMWUT*, vol. 2, no. 1, p. 41, 2018.

[45] J. Han, C. Qian, Y. Yang, G. Wang, H. Ding, X. Li, and K. Ren, "Butterfly: Environment-independent physical-layer authentication for passive rfid," *ACM IMWUT*, vol. 2, no. 4, p. 166, 2018.

[46] P. Li, Z. An, L. Yang, P. Yang, and Q. Lin, "Rfid harmonic for vibration sensing," *IEEE Transactions on Mobile Computing*, vol. 20, no. 4, pp. 1614–1626, 2019.

[47] C. Wang, L. Xie, W. Wang, Y. Chen, Y. Bu, and S. Lu, "Rf-ecg: Heart rate variability assessment based on cots rfid tag array," *ACM IMWUT*, vol. 2, no. 2, p. 85, 2018.

[48] H. Jin, J. Wang, Z. Yang, S. Kumar, and J. Hong, "Rf-wear: Towards wearable everyday skeleton tracking using passive rfids," in *ACM Ubicomp*, 2018, pp. 369–372.

[49] L. Yang, Q. Lin, X. Li, T. Liu, and Y. Liu, "See through walls with cots rfid system!" in *ACM MobiCom*, 2015, pp. 487–499.

[50] Z. Wang, F. Xiao, N. Ye, R. Wang, and P. Yang, "A see-through-wall system for device-free human motion sensing based on battery-free rfid," *ACM Transactions on Embedded Computing Systems*, vol. 17, no. 1, p. 6, 2018.

[51] H. Ding, C. Qian, J. Han, G. Wang, W. Xi, K. Zhao, and J. Zhao, "Rfipad: Enabling cost-efficient and device-free in-air handwriting using passive tags," in *IEEE ICDCS*, 2017, pp. 447–457.

[52] Y. Zou, J. Xiao, J. Han, K. Wu, Y. Li, and L. M. Ni, "Grfid: A device-free rfid-based gesture recognition system," *IEEE Transactions on Mobile Computing*, vol. 16, no. 2, pp. 381–393, 2016.

[53] J. Wang, J. Xiong, X. Chen, H. Jiang, R. K. Balan, and D. Fang, "Tagscan: Simultaneous target imaging and material identification with commodity rfid devices," in *ACM MobiCom*, 2017, pp. 288–300.

[54] C. Yang, X. Wang, and S. Mao, "Sparsetag: High-precision backscatter indoor localization with sparse rfid tag arrays," in *IEEE SECON*, 2019, pp. 1–9.

[55] C. A. Balanis, *Antenna theory: analysis and design*. John wiley & sons, 2016.

[56] S. E. Asl, M. T. Ghasr, M. Zawodniok, and K. E. Robinson, "Preliminary study of mutual coupling effect on a passive rfid antenna array," in *IEEE International Instrumentation and Measurement Technology Conference*, 2013, pp. 138–141.

[57] J. Machac, A. Boussada, M. Svanda, J. Havlicek, and M. Polivka, "Influence of mutual coupling on stability of rcs response in chipless rfid," *Technologies*, vol. 6, no. 3, p. 67, 2018.

[58] F. Lu, X. Chen, and T. Y. Terry, "Performance analysis of stacked rfid tags," in *IEEE International Conference on RFID*, 2009, pp. 330–337.
[59] S. Caizzone, E. DiGiampaolo, and G. Marrocco, "Wireless crack monitoring by stationary phase measurements from coupled rfid tags," *IEEE Transactions on Antennas and Propagation*, vol. 62, no. 12, pp. 6412–6419, 2014.

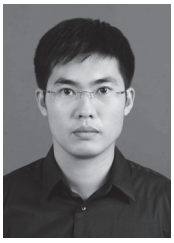

Zhongqin Wang received his M.S. degrees from Nanjing University of Posts and Telecommunications, Nanjing, China in 2014, and Ph.D. degree from University of Technology Sydney, Australia in 2020, all in computer science. He worked as a research engineer from 2020 to 2021 in University of Technology Sydney, Australia. He is a Lecturer in the College of Information and Engineering, Capital Normal University, Beijing, China. His research interest includes Wireless Sensing based on RFID, WiFi and mmWave.

Dr J. Andrew Zhang (M'04-SM'11) received B.Sc. degree from Xi'an JiaoTong University, China, in 1996, M.Sc. degree from Nanjing University of Posts and Telecommunications, China, in 1999, and Ph.D. degree from the Australian National University, in 2004. Currently, He is an Associate Professor in the School of Electrical and Data Engineering, University of Technology Sydney, Australia. Dr. Zhang's research interests are in the area of signal processing for wireless communications and sensing, and autonomous vehicular networks. He has published 200+ journal and conference papers, and has won 5 best paper awards.

Fu Xiao Fu Xiao received the Ph.D degree in Nanjing University of Science and Technology, Nanjing, China in 2007. He is currently a professor and Ph.D supervisor in the School of Computer, Nanjing University of Posts and Telecommunications, Nanjing, China. His main research interest is Wireless Sensor Networks. Dr. Xiao is a member of the IEEE Computer Society and the Association for Computing Machinery.

Min Xu (M'10) is currently an Associate Professor at University of Technology Sydney. She received the B.E. degree from the University of Science and Technology of China, Hefei, China, in 2000, the M.S. degree from National University of Singapore, Singapore, in 2004, and the Ph.D. degree from University of Newcastle, Callaghan NSW, Australia, in 2010. Her research interests include multimedia data analytics, computer vision and machine learning. She has published over 100 research papers in high quality international journals and conferences. She has been invited to be a member of the program committee for many international top conferences, including ACM Multimedia Conference and reviewers for various highly-rated international journals, such as IEEE Transactions on Multimedia, IEEE Transactions on Circuits and Systems for Video Technology and much more. She is an Associate Editor of Journal of Neurocomputing.